
Article:
Li, W., Long, L., Yang, X. et al. (20 more authors) (2021) Circulating BMP9 protects the pulmonary endothelium during inflammation-induced lung injury in mice. American Journal of Respiratory and Critical Care Medicine, 203 (11). pp. 1419-1430. ISSN 1073-449X

https://doi.org/10.1164/rccm.202005-1761oc

Circulating BMP9 protects the pulmonary endothelium during inflammation-induced lung injury in mice

Wei Li, Ph.D.[1,*,$], Lu Long, Ph.D.[1], Xudong Yang, Ph.D.[1], Zhen Tong, Ph.D.[1], Mark Southwood, Ph.D.[1], Ross King, Ph.D.[2], Paola Caruso, Ph.D.[1], Paul D Upton, Ph.D.[1], Peiran Yang, Ph.D.[3], Geoffrey A Bocobo, B.Sc.[3], Ivana Nikolic, M.D.[4], Angelica Higuera, M.D.[5], Richard M Salmon, Ph.D.[1], He Jiang, M.Sc.[1], Katharine M Lodge, M.D., Ph.D.[6], Kim Hoenderdos, Ph.D.[1], Rebecca M Baron, M.D.[5], Paul B Yu, M.D., Ph.D[3], Alison M Condliffe, M.D., Ph.D.[7], Charlotte Summers, M.D., Ph.D.[1], Sussan Nourshargh, Ph.D.[2], Edwin R Chilvers, Ph.D., FRCP[6], Nicholas W Morrell, M.D., Ph.D.[1,*,$]

ORCIDs:

Wei Li: 0000-0002-1924-3120

Zhen Tong: 0000-0002-9321-3165

Mark Southwood: 0000-0002-3493-9599

Ross King: 0000-0002-4819-9464

Paola Caruso: 0000-0002-3071-1917

Paul D Upton: 0000-0003-2716-4921

Peiran Yang: 0000-0002-4635-1215

Geoffrery A Bocobo: 0000-0002-7392-5376

Angelica Higuera: 0000-0001-9753-3089

Richard M Salmon: 0000-0001-6327-5341

Katharine M Lodge: 0000-0002-3203-9941

Paul B Yu: 0000-0003-2145-4944

Alison M Condliffe: 0000-0002-6697-8648

Charlotte Summers: 0000-0002-7269-2873

Sussan Nourshargh: 0000-0001-5677-1806

Edwin R Chilvers: 0000-0002-4230-9677

Nicholas W Morrell: 0000-0001-5700-9792

Running title*:* The role and regulation of endogenous BMP9

[1]Department of Medicine, University of Cambridge, School of Clinical Medicine, Cambridge, UK.

[2]William Harvey Research Institute, Barts and the London School of Medicine & Dentistry, Queen Mary University of London, London, UK.

[3&5]Cardiovascular Medicine Division[3] and Division of Pulmonary and Critical Care Medicine[5], Department of Medicine, Brigham and Women's Hospital, Harvard Medical School, Boston, Massachusetts, USA.

[4]Cardiovascular Medicine Division, Department of Medicine, Massachusetts General Hospital, Boston, MA, USA

[6]National Heart and Lung Institute, Imperial College London, London, UK.

[7]Department of Infection, Immunity & Cardiovascular Disease, University of Sheffield, Sheffield, UK.

[*] Joint senior authors

[$]Corresponding Authors:

Dr. Wei Li, Email: wl225@cam.ac.uk, Tel: +44 (0) 1223 761304, Department of Medicine, University of Cambridge, Level 5, Addenbrooke's Hospital, Box 157, Hills Road, Cambridge, CB2 0QQ

Prof. Nicholas W Morrell, Email: nwm23@cam.ac.uk, Tel: +44 (0) 1223 331666, Department of Medicine, University of Cambridge, Level 5, Addenbrooke's Hospital, Box 157, Hills Road, Cambridge, CB2 0QQ

Conflict of Interest. WL and PDU are founders and consultants to Morphogen-IX. NWM is a founder and CEO of Morphogen-IX.

Author Contributions: LL, XY and RK designed and performed all the *in vivo* experiments. MS performed all the histological analysis. WL, PC, ZT, PDU, RMS, HJ, KML and KH performed the biochemical, cell biology and animal tissue sample measurements. PY, GAB, IN, RMB, AH collected the plasma samples and measured BMP9 levels in the human subjects' plasma. WL and NWM conceived the idea, designed the study. WL, RMB, PBY, AMC, CS, SN, ERC and NWM supervised the experiments and wrote the manuscript.

Funding: This work was supported by the following grants: British Heart Foundation grants (PG/17/1/32532 to WL and NWM, PG/17/58/33134 to WL, NWM and CS, CH/09/001/25945 and RG/13/4/30107 to NWM, PG/14/62/31034 to SN), the Wellcome Trust grant (098291/Z/12/Z to SN), MRC grant (MR/K020919/1 to NWM), British Lung Foundatin grant (BLF COPD10/5 to AMC), and National Institutes of Health Grants (P01-HL108801 to RMB, R01-HL131910 to PBY and R42-HL132742 to PBY). KML was supported by a Wellcome Trust Clinical Research Fellowship (102706/Z/13/Z). Infrastructure support was provided by the Cambridge NIHR Biomedical Research Centre.

Subject descriptor: 4.1 ALI/ARDS: Biological Mechanisms

Short summary:

Scientific Knowledge on the Subject: Increased pulmonary endothelial permeability is a major factor in the development of acute respiratory distress syndrome (ARDS). Evidence is emerging that circulating BMP9, secreted from the liver, might protect the pulmonary endothelium from

injury. For example, loss of BMP9 levels or its signalling receptor contributes to the development of pulmonary arterial hypertension. The role of endogenous BMP9 in endothelial permeability remains unclear.

What This Study Adds to the Field: Here we show that subacute neutralization of endogenous BMP9 leads to lung vascular injury, including enhanced endothelial permeability and neutrophil extravasation. BMP9 levels were markedly reduced in the setting of inflammation in mice and humans. Conversely, exogenous supplementation of BMP9 protected the lung from LPS-induced injury. This study suggests that exogenous BMP9 could offer a novel approach to prevent increased pulmonary endothelial permeability in the setting of lung injury and ARDS.

Total word count: 3499 **words**

This article has an online data supplement.

ABSTRACT

Rationale: Pulmonary endothelial permeability contributes to the high-permeability pulmonary edema that characterizes acute respiratory distress syndrome (ARDS). Circulating bone morphogeneic protein 9 (BMP9) is emerging as an important regulator of pulmonary vascular homeostasis.

Objective: To determine whether endogenous BMP9 plays a role in preserving pulmonary endothelial integrity, and whether loss of endogenous BMP9 occurs during lipopolysacharride (LPS) challenge.

Methods: A BMP9-neutralizing antibody was administrated to healthy adult mice and lung vasculature was examined. Potential mechanisms were delineated by transcript analysis in human lung endothelial cells. Impact of BMP9 administration was evaluated in a murine acute lung injury model induced by inhaled LPS. Levels of BMP9 were measured in plasma from patients with sepsis and endotoxemic mice.

Main Results: Subacute neutralization of endogenous BMP9 in mice (N=12) resulted in increased lung vascular permeability (P=0.022), interstitial edema (P=0.0047) and neutrophil extravasation (P=0.029) compared with IgG control (N=6). In pulmonary endothelial cells, BMP9 regulated transcriptome pathways implicated in vascular permeability and cell membrane integrity. Augmentation of BMP9 signaling in mice (N=8) prevented inhaled LPS-induced lung injury (P=0.0027) and edema (P<0.0001). In endotoxemic mice (N=12), endogenous BMP9 levels were markedly reduced, due to a transient reduction in hepatic BMP9 mRNA expression and increased elastase activity in plasma. In human sepsis patients (N=10), circulating levels of BMP9 were also markedly reduced (P<0.0001).

Conclusions: Endogenous circulating BMP9 is a pulmonary endothelial protective factor, down-regulated during inflammation. Exogenous BMP9 offers a potential therapy to prevent increased pulmonary endothelial permeability in lung injury.

(Word count: 245/250)

Keywords:

BMP9, BMP signalling in endothelial cells, Pulmonary endothelium, Lung injury

INTRODUCTION

Endothelial dysfunction, inflammation and increased capillary permeability play central roles in the pathobiology of sepsis and the acute respiratory distress syndrome (ARDS)(1). Previous studies have identified important signaling pathways and protein-protein interactions within inter-endothelial junctions that regulate endothelial barrier function(2). However, such knowledge has not yet resulted in approved drugs that target the increased vascular permeability present in sepsis and ARDS(1), conditions associated with an unacceptably high mortality. Exploring new pathways that preserve endothelial integrity may hasten the discovery of novel approaches to the treatment of these conditions.

Bone morphogenetic protein 9 (BMP9) is a member of the transforming growth factor β (TGFβ) family that signals selectively in endothelial cells via a receptor complex comprising the high affinity type 1 BMP receptor activin receptor-like kinase 1 (ALK1), and the type 2 BMP receptors, BMP receptor type II (BMPRII) or activin receptor type 2A(3-5). ALK1 is expressed almost exclusively on endothelial cells(6), and its expression is 10 to 200-fold higher in lung compared to other tissues, indicating a particular role for ALK1-mediated signaling in homeostasis of the pulmonary endothelium(7). We previously show that BMP9 protects human pulmonary artery endothelial cells (hPAECs) against excessive permeability induced by TNF, LPS or thrombin(8). Moreover, administration of recombinant BMP9 protected mice against Evans Blue (EB) extravasation in the lung following intraperitoneal LPS challenge(8). Recently, adenoviral delivery of BMP9 was shown to prevent retinal vascular permeability in diabetic mice(9). Despite such evidence suggesting that augmentation of BMP9 signaling might prevent endothelial hyperpermeability, the role and regulation of endogenous BMP9 in the maintainence of endothelial barrier function have not been investigated.

BMP9 is synthesized predominantly in the liver(10), circulates at levels that constitutively activate endothelial ALK1 signaling, and comprises the majority of plasma BMP activity(11). Heterozygous deleterious mutations in the *GDF2* gene (which encodes for BMP9) have been reported in patients with pulmonary arterial hypertension (PAH)(12-15) and result in reduced circulating levels of BMP9. Furthermore, reduced levels of plasma BMP9 are found in patients with cirrhosis and portopulmonary hypertension(16, 17). Interestingly, increased vascular permeability is a well recognized feature of chronic cirrhosis.

Given the potential protective effect of BMP9 signaling in the pulmonary endothelium, we sought to determine whether endogenous BMP9 plays a role in protecting the pulmonary endothelium and whether inflammation regulates endogenous BMP9. We further explored the potential of exogenous BMP9 as a lung vascular protective agent in the setting of acute lung injury (ALI). Some of these results have been previously reported in the form of abstracts(18-20).

MATERIALS AND METHODS

Human Samples. Human plasma samples were obtained from a prospectively enrolled cohort of patients admitted to the adult medical intensive care unit (MICU) Registry of Critical Illness, and healthy human volunteers without known cardiopulmonary disease, in accordance with the Institutional Review Board–approved protocol at Brigham and Women's Hospital as described previously(21-23). Written informed consent was obtained from all participants or their appropriate surrogates.

Animal procedures. All procedures were carried out in accordance with the Home Office Animals (Scientific Procedures) Act 1986 and approved under Home Office Project Licences 80/2460 and 70/8850 to N.W.M and and PPL 7007884 to S.N.

Murine endotoxemia studies. Mice were injected intraperitoneally with 2 mg/kg LPS or vehicle. After the length of time as specified in figure legends, mice were sacrificed using ketamine (100 mg/kg) and xylazine (10 mg/kg). Detailed tissue harvests and measurements can be found in the online data supplement. N=6 for each time point in LPS-treated groups. For PBS-treated controls, 3 animals were included at 0, 6, 18 and 24 hours respectively, and pooled for the final analysis (final N=12 in PBS-treated group).

BMP9 ELISA. BMP9 ELISA was carried out as described previously(13, 16).

Anti-BMP9 treatment in mice. Mice were injected intraperitoneally with 5 mg/kg anti-BMP9 antibody (N=12), or murine IgG2B isotype control (N=6) on Day 0 and Day 2 and lung vascular permeability was measured on Day 3 using the EB dye extravasation assay as described previously(8) (Figure 1A). Separate groups of control mice were injected intraperitoneally with LPS at 1.5 (LPS1) or 3 mg/kg (LPS2) (both N=6), or PBS control (N=12) on Day 2 and permeability was measured on Day 3. Half of the lung tissues were harvested for measuring vascular permeability, and the other half were inflated and fixed in formalin and processed into paraffin wax blocks for histological analysis.

Murine inhaled LPS model. Mice were injected intraperitoneally with either PBS or BMP9 (at 1.5 μg/kg, N=8 per group) 1 hour before being challenged with 20 μg/mouse LPS in PBS via the intranasal route. After 24 hours, one lung was harvested for quantification of EB dye extravasation. The other lung was saved for histological analysis, and for RNA extraction/qPCR analysis.

Statistical analysis. All *in vitro* experiments were conducted at least three times, and representative images are shown. Data analysis was performed using GraphPad Prism 6. Results are shown as means ± SEM. Statistical significance was analyzed by two-tailed non-parametric tests or One-way ANOVA as indicated in figure legends. Values of $P < 0.05$ were considered significant.

Expanded Materials and Methods can be found in the online data supplement. Microarray data have been deposited to Gene Expression Omnibus, with the accession number of GSE118353.

RESULTS

Inhibition of endogenous BMP9 increases lung vascular permeability and neutrophil extravasation

Following the protocol shown in Figure 1A, mice treated with anti-BMP9 antibody exhibited significantly higher levels of EB dye in their lungs compared with mice treated with control IgG (Figure 1B), although EB leak was only observed in the higher LPS dose group (Figure 1B, LPS2). Histology of lung tissue demonstrated marked perivascular edema in mice exposed to either anti-BMP9 or LPS (Figure 1C, black arrows). Morphometry of arteries associated with terminal bronchioles confirmed acellular expansion of the adventitia, which correlated with the magnitude of EB dye accumulation in the lung (Figure 1D). Unexpectedly, anti-BMP9-treated mice showed a significant accumulation of neutrophils in the alveolar space, similar to that observed in LPS-treated animals (Figure 1E). To confirm that the anti-BMP9 antibody had inhibited circulating BMP9 activity, we tested plasma BMP activity by monitoring its ability to induce *ID1* gene expression in hPAECs(10, 24, 25). Indeed, plasma from anti-BMP9 treated animals showed reduced BMP activity, as evidenced by significantly lower *ID1* mRNA induction compared with plasma from IgG-treated controls (Figure 1F).

To evaluate whether the effect of anti-BMP9 is specific to the pulmonary vasculature, we performed intravital microscopy imaging of the mouse cremaster microvessels to directly visualize the effects of neutralizing endogenous BMP9 under physiological conditions. Within 5 minutes of administrating anti-BMP9 antibody via the tail vein, we observed a marked increase in the extravasation of TRITC-Dextran from post-capillary venules of the cremaster muscle

compared with the IgG control group (Figure E1 A-C). The rapidity and magnitude of this response were similar to that induced by histamine (Figure E1 D). This confirms that loss of endogenous of BMP9 leads to excess vascular leak and this effect is not limited to the pulmonary circulation.

BMP9 signaling regulates key pathways involved in endothelial cell membrane integrity and permeability

To elucidate potential mechanisms by which BMP9 might act as an endothelial protective factor, we performed a microarray analysis of global differential gene expression in hPAECs in response to BMP9. We used the prodomain-bound form of BMP9 (pro-BMP9) which is the circulating form(11), at a concentration representative of those measured in healthy human plasma(16, 26), and exposed hPAECs for 5 hours. Using a threshold adjusted P-value of 0.05 as a cutoff, BMP9 upregulated the expression of 30 genes and downregulated 85 genes (Table E1&E2). However, the continuum changes in the adjusted P-values for both up- and down-regulated genes indicate that more transcripts are likely to be regulated than those passing this threshold (Figure 2A). Pathway analysis showed that BMP9-regulated pathways include TGFβ signaling , cytokine-cytokine receptor interaction and Rap1 signaling (Table E3&E4). Cellular component gene ontology (GO) analysis revealed that BMP9 regulated genes are highly enriched in the plasma membrane and extracellular space (Figure E2 and Table E5). As expected, BMP9 increased the expression of *BMPR2* and *ID1*(3) (Figure 2A). Of the genes known to regulate endothelial permeability, pro-BMP9 treatment down-regulated *AQP1* (encoding aquaporin-1) and *KDR* (encoding VEGFR2), and up-regulated *TEK* (encoding Tie2) (Figure 2A), which were further validated by RT-qPCR analysis (Figure 2B).

Next we performed the converse experiments by selectively neutralizing BMP9 in serum from FBS-containing endothelial growth media. Reciprocal changes in gene expression, i.e. a

significant increase in *AQP1* and *KDR* expression and a reduction in *TEK* expression, were obtained (Figure 2C), supporting that endogenous serum BMP9 regulates these genes even in the presence of other serum factors. Immunoblotting confirmed that BMP9-treatment reduced VEGFR2 protein levels (Figure 2D). AQP1 expression in cultured PAECs was too low to be robustly detected by western blotting.

Since the lung microvascular endothelium rather than the conduit artery endothelium is involved in lung hyperpermeability, we further examined responses in human pulmonary microvascular endothelial cells (hPMECs). Pro-BMP9 signalled more potently in hPMECs (EC_{50} = 7.2 ± 1.5 pg/ml) compared with hPAECs (EC_{50} = 81 ± 23 pg/ml, Figure E3A), and robustly induced known BMP9-target genes such as *ID1* and *BMPR2* (Figure E3B). BMP9 treatment also suppressed *AQP1* and *KDR* expression, and induced *TEK* expression in hPMECs (Figure 2E). Functionally, anti-BMP9 treatment in PMECs led to enhanced apoptosis (Figure 2F) and increased permeability (Figure 2G) compared with IgG-treated controls. Knockdown of *BMPR2* by siRNA reversed the protection by BMP9 from LPS-induced leak in PMEC monolayer (Figure E3C). Consistent with these observations, we also observed loss of VE-cadherin junctions when hPAECs were treated with anti-BMP9 antibody (Figure E4). Taken together, these data strongly support a role of BMP9 signaling in protecting endothelial cell membrane integrity and barrier function.

Exogenous BMP9 protects mice from ALI in response to inhaled LPS

Acute inhalation of LPS initiates epithelial cell damage and causes lung vascular hyperpermeability and injury. To further explore the potential therapeutic value of BMP9(8), we questioned whether administration of exogenous BMP9 prevents ALI in such a murine model. As expected, inhalation of LPS led to pulmonary inflammation and congestion (Figure 3A) and increased lung vascular permeability measured by extravasation of EB dye (Figure 3B). All of

these features were completely prevented by pre-treating mice with BMP9. The degree of lung injury was scored following the recommendation of the American Thoracic Society workshop report(27) (Figure 3C), and the number of neutrophils extravasated into alveoli were counted (Figure 3D). Supplementation of BMP9 resulted in a complete protection against LPS-induced lung injury and neutrophil extravasation. Interestingly, in this model, plasma levels of neutrophil elastase were also elevated following LPS-treatment and this increase was prevented in the BMP9 pre-treated animals (Figure 3E), suggesting an anti-inflammatory role of BMP9. To confirm target engagement, we measured the changes in BMP9-regulated genes in the lung. As expected, administration of BMP9 led to an enhancement in BMP signaling, as evidenced by the elevated mRNA expression of the BMP9 target genes *Id1* and *Bmpr2* (Figure 3F&G). Of note, consistent with the results from *in vitro* studies (Figure 2), the expression of *Tek* (Tie2) was significantly reduced following LPS challenge, and restored by BMP9 treatment (Figure 3H). Furthermore, LPS treatment led to a 2-fold increase in expression of *Kdr* (VEGFR2), which was completely prevented by the pre-treatment with BMP9 (Figure 3I).

Plasma BMP9 is suppressed during endotoxemia

Given that both depletion or supplementation of BMP9 impacts lung vascular permeability, we questioned whether circulating BMP9 levels are reduced *per se* in the setting of systemic inflammation in humans and mice. Eighteen hours after intraperitoneal LPS administration, mice exhibited a systemic inflammatory response, as evidenced by a reduction in platelet numbers and an increase in alveolar neutrophil counts (Figure E5 A&B). Concentrations of neutrophil elastase were significantly elevated in both plasma and bronchoalveolar lavage fluid (BALF, Figure E5 C&D). As hypothesized, circulating levels of BMP9 were markedly decreased in this murine model (Figure 4A).

To further delineate changes in the endogenous BMP9 during inflammation, we performed a time-course study to track the mRNA and protein changes in BMP9 following the onset of endotoxemia in mice. Plasma BMP9 levels decreased from 6 hours after LPS exposure and continued to fall at the 24-hour time point (Figure 4B). Hepatic *Bmp9* mRNA levels were suppressed by ~80% at 3 hours post LPS exposure (Figure 4C), but returned to control values by 18 hours, despite the continued reduction in plasma BMP9 levels at these time points. As comparators, we measured liver mRNA levels for IL-6 to monitor the inflammatory response, and BMP6, another BMP known to be expressed in the liver(28). There was a sharp increase in *Il6* mRNA at 45 minutes after LPS administration, which fell at 3 hours and returned to baseline levels at 18 hours (Figure 4D). *Bmp6* mRNA was reduced to ~60% of the control levels by 3 hours and remained suppressed throughout the 24 hour period (Figure 4E). These comparators confirm that the transient reduction of *Bmp9* mRNA levels is unique for BMP9 and not due to the global suppression and recovery of mRNA synthesis in the liver.

Since the continued reduction in plasma BMP9 during mouse endotoxemia could not be explained fully by the changes in hepatic *Bmp9* mRNA alone, we investigated whether BMP9 might also be degraded by plasma proteases. Inflammation leads to the activation of neutrophils, which release large amounts of proteases, especially elastase(29); we therefore investigated whether LPS challenge causes changes in circulating neutrophil elastase (NE) levels. Compared with PBS-treated control animals, administration of LPS caused a 10-fold increase in plasma elastase concentration at 45 minutes, and an 80-fold increase at 24 hours (Figure 4F). Because α1-antitrypsin (AAT) is the major NE inhibitor in plasma(30), we also measured AAT liver mRNA and plasma protein levels. AAT mRNA levels were largely unchanged over the first 6 hours but decreased to about 50% of controls at 18 and 24 hours (Figure E6 A). Using an ELISA that specifically detects the native and active form of AAT (Figure E6 B)(31), we observed that plasma levels of active AAT were largely unchanged throughout the 24-hour time course following LPS

challenge (Figure 4F). This indicated that the 80-fold increase in NE levels was not counteracted by a similar fold increase in this endogenous inhibitor, leading to an imbalance favoring heightened elastase activity during endotoxemia. To examine whether circulating BMP9 levels are reduced in patients with systemic inflammatory response syndrome (SIRS) and sepsis, plasma BMP9 levels were measured in 10 patients with SIRS, 10 patients with sepsis, all sampled within 72 hours of admission to the MICU, and 10 age- and sex-matched healthy controls. The clinical characteristics and the demographics of the subjects are summarized in Table E6 and are notable for the presence of positive microbiology cultures and an increased reliance upon vasopressors for blood pressure support in the sepsis patients compared with the other groups. Importantly, plasma BMP9 levels were significantly reduced in patients with SIRS and further reduced in sepsis, compared with healthy controls (Figure 4G).

BMP9 is a substrate for neutrophil elastase

Finally we sought to confirm whether BMP9 can be cleaved by NE. Using purified recombinant proteins, pro-BMP9 can be cleaved efficiently by NE, despite being highly resistant to trypsin digestion (Figure 5A). Next, we questioned whether NE in plasma could contribute to BMP9 cleavage, since primed circulating neutrophils (with increased capacity for systemic degranulation) were identified in ARDS patients(32), activated neutrophils release a number of proteases upon degranulation(29), and significantly higher levels of NE were found in plasma from endotoximic mice (Figure 4F). Purified human peripheral blood neutrophils were activated *in vitro* to degranulate and release proteases into the culture supernatant as described previously(29) (Figure 5B). Pro-BMP9 was incubated with supernatants derived from activated neutrophils, in the presence or absence of a panel of protease inhibitors (PI). Activated neutrophil supernatants cleaved BMP9 effectively and this process was blocked by AAT and sivelestat, a selective NE inhibitor (Figure 5 C&D), but not by the chelating agent EDTA,

suggesting that metalloproteases do not play a role. Taken together these findings suggest that NE contributes to BMP9 cleavage in the settting of inflammation.

DISCUSSION

The present study provides evidence that endogenous BMP9 is an important protective factor for the pulmonary vascular endothelium that is down-regulated during inflammation. Selective inhibition of circulating BMP9 induced heightened lung vascular leak. Such a finding is consistent with reports that ALK1-Fc, a ligand trap of BMP9, causes peripheral edema as a common side effect in clinical trials(33, 34). In addition, loss of the major type 2 receptor for BMP9, BMPR-II, promotes endothelial permeability and contributes to the development of PAH(8, 35). Since ALK1 is particularly highly expressed on lung vascular endothelium(7), we speculate that the pulmonary circulation is particularly dependent on BMP9/ALK1 signaling to maintain barrier function.

Emerging roles of BMP signaling in vascular biology, particularly in endothelial cells, have been recognized and reviewed recently(36). There may be important context-specific differences in the roles of specific BMPs in the regulation of endothelial barrier function. For example, there is evidence that specific BMPs, including BMP2, BMP4 and BMP6 (37-39), destabilize endothelial cell junctions to increase vascular permeability. On the other hand, recombinant BMP2 and BMP4 have also been shown to play a protective role in endotoxin-induced ALI (40, 41). BMP 2, 4 and 6 must act through different mechanisms to BMP9 since only BMP9 and BMP10 signal specifically through the ALK1-mediated pathway in vascular endothelial cells.

The circulating form of BMP9 at physiological concentrations regulates the transcription of gene sets highly associated with the plasma membrane and extracellular space. This is consistent with previous findings either using BMP9-treated human dermal microvascular endothelial cells(42), or comparing wild type versus *Bmpr2*$^{\text{-kncokout}}$ endothelial cells(43). Among the BMP9-regulated

genes are three receptors controlling critical pathways involved in endothelial permeability. Importantly, we show that *in vivo*, the protection by BMP9 against lung vascular leak in a murine ALI model was associated with the preservation of *TEK* and *KDR* expression in the LPS-exposed lungs. The effect of VEGF signaling via VEGFR2 to induce vascular leak has been extensively studied(44). Consistent with a role for Tie2, increased expression of angiopoietin 2 was found in the retina of neonatal mice receiving anti-BMP9 and anti-BMP10 antibodies(45). AQP1 regulates osmotically-driven water transport across microvessels in adult lungs and facilitates hydrostatically-driven lung edema(46). Decreased pulmonary vascular permeability has been described in *AQP1*-null humans(47) and *AQP1* expression is increased in the capillary endothelium of alveoli from patients with ARDS(48).

It is interesting to note the inverse correlation of circulating BMP9 and elastase concentrations in the onset of endotoxemia in mice, and that BMP9 is a direct substrate of NE *in vitro* despite it being highly resistant to trypsin digestion. Further experiments are needed to show BMP9 cleavage by NE *in vivo*. This could be challenging because we show here that NE is a major but not the only serine protease released by neutrophils that has the ability to cleave BMP9 (Figure 5C&D), therefore elastase inhibition alone may not be enough to rescue BMP9 levels in the circulation. A direct detection of elastase-cleaved BMP9 fragments *in vivo* would be more informative, however, this is difficult due to the presence of very low concentrations of BMP9 in the circulation (200-400 pg/ml).

LPS challenge causing a temporary down regulation in BMP9 mRNA in the liver is consistent with a previous report that BMP9 expression is transiently reduced in three models of acute liver damage(49). Interestingly, in another study examining the changes of BMP signaling pathways after acute LPS challenge, a similar transient down-regulation of Smad1/5 phosphorylation, Id1 proteins and Bmp4 mRNA was observed in the lung tissue(50).

We previously reported that BMP9 enhances LPS-induced leukocyte recruitment to the vascular endothelium(51). This effect was observed with higher concentrations of BMP9 that likely activates the ALK2 receptor(52). The present study used lower concentrations of BMP9, and data in this study are consistent with the results reported by Burton *et al*(35) and Long *et al*(8) . Since BMP9 can signal through both the high affinity receptor ALK1 and the low affinity receptor ALK2, our overall results suggest that restoration of BMP9 levels to the physiological concentration range will promote BMP9 to signal through the ALK1-mediated pathway and exert beneficial anti-inflammatory and endothelial-protective effects.

Microvascular leak has now been recognized as a major contributor to septic shock and is associated with increased morbidity and mortality; as yet, there is no pharmacological drug available that targets this process(53). Restoration of endothelial integrity has been shown to increase survival in three different animal models of systemic inflammation(54). Our study identifies a new and unexpected essential role for endogenous BMP9 in the maintenance of endothelial barrier function under physiological conditions, and demonstrates that circulating BMP9 levels are reduced in sepsis patients and in a murine endotoxemia model. Importantly, administration of BMP9 protects against lung vascular leak in a murine ALI model. Taken together, these findings support the exploration of BMP9 as a biomarker as well as a potential therapy for the prevention of vascular permeability and lung injury associated with sepsis and ARDS.

ACKNOWLEDGEMENTS

We are grateful to Dr James Thaventhiran for providing training on the inhaled LPS procedure, MICU Registry members Laura Fredenburgh, Paul Dieffenbach, Samuel Ash at Brigham and Women's Hospital for collecting human plasma samples. We also thank the support from

Cambridge Genomic Service, in particular Dr. Emily Clemente and Dr. Julien Bauer, for the microarray data analysis.

REFERENCES:

1. Millar FR, Summers C, Griffiths MJ, Toshner MR, Proudfoot AG. The pulmonary endothelium in acute respiratory distress syndrome: insights and therapeutic opportunities. *Thorax* 2016; 71: 462-473.

2. Komarova YA, Kruse K, Mehta D, Malik AB. Protein Interactions at Endothelial Junctions and Signaling Mechanisms Regulating Endothelial Permeability. *Circ Res* 2017; 120: 179-206.

3. David L, Mallet C, Mazerbourg S, Feige JJ, Bailly S. Identification of BMP9 and BMP10 as functional activators of the orphan activin receptor-like kinase 1 (ALK1) in endothelial cells. *Blood* 2007; 109: 1953-1961.

4. Scharpfenecker M, van Dinther M, Liu Z, van Bezooijen RL, Zhao Q, Pukac L, Lowik CW, ten Dijke P. BMP-9 signals via ALK1 and inhibits bFGF-induced endothelial cell proliferation and VEGF-stimulated angiogenesis. *J Cell Sci* 2007; 120: 964-972.

5. Upton PD, Davies RJ, Trembath RC, Morrell NW. Bone morphogenetic protein (BMP) and activin type II receptors balance BMP9 signals mediated by activin receptor-like kinase-1 in human pulmonary artery endothelial cells. *J Biol Chem* 2009; 284: 15794-15804.

6. Seki T, Yun J, Oh SP. Arterial endothelium-specific activin receptor-like kinase 1 expression suggests its role in arterialization and vascular remodeling. *Circ Res* 2003; 93: 682-689.

7. Panchenko MP, Williams MC, Brody JS, Yu Q. Type I receptor serine-threonine kinase preferentially expressed in pulmonary blood vessels. *Am J Physiol* 1996; 270: L547-558.

8. Long L, Ormiston ML, Yang X, Southwood M, Graf S, Machado RD, Mueller M, Kinzel B, Yung LM, Wilkinson JM, Moore SD, Drake KM, Aldred MA, Yu PB, Upton PD, Morrell NW. Selective enhancement of endothelial BMPR-II with BMP9 reverses pulmonary arterial hypertension. *Nat Med* 2015; 21: 777-785.

9. Akla N, Viallard C, Popovic N, Lora Gil C, Sapieha P, Larrivee B. BMP (Bone Morphogenetic Protein) 9/Alk1 (Activin-Like Kinase Receptor Type I) Signaling Prevents Hyperglycemia-Induced Vascular Permeability. *Arterioscler Thromb Vasc Biol* 2018.

10. David L, Mallet C, Keramidas M, Lamande N, Gasc JM, Dupuis-Girod S, Plauchu H, Feige JJ, Bailly S. Bone morphogenetic protein-9 is a circulating vascular quiescence factor. *Circ Res* 2008; 102: 914-922.

11. Bidart M, Ricard N, Levet S, Samson M, Mallet C, David L, Subileau M, Tillet E, Feige JJ, Bailly S. BMP9 is produced by hepatocytes and circulates mainly in an active mature form complexed to its prodomain. *Cell Mol Life Sci* 2012; 69: 313-324.

12. Graf S, Haimel M, Bleda M, Hadinnapola C, Southgate L, Li W, Hodgson J, Liu B, Salmon RM, Southwood M, Machado RD, Martin JM, Treacy CM, Yates K, Daugherty LC, Shamardina O, Whitehorn D, Holden S, Aldred M, Bogaard HJ, Church C, Coghlan G, Condliffe R, Corris PA, Danesino C, Eyries M, Gall H, Ghio S, Ghofrani HA, Gibbs JSR, Girerd B, Houweling AC, Howard L, Humbert M, Kiely DG, Kovacs G, MacKenzie Ross RV, Moledina S, Montani D, Newnham M, Olschewski A, Olschewski H, Peacock AJ, Pepke-Zaba J, Prokopenko I, Rhodes CJ, Scelsi L, Seeger W, Soubrier F, Stein DF, Suntharalingam J, Swietlik EM, Toshner MR, van Heel DA, Vonk Noordegraaf A, Waisfisz Q, Wharton J, Wort SJ, Ouwehand WH, Soranzo N, Lawrie A, Upton PD, Wilkins MR, Trembath RC, Morrell NW. Identification of rare sequence variation underlying heritable pulmonary arterial hypertension. *Nat Commun* 2018; 9: 1416.

13. Hodgson J, Swietlik EM, Salmon RM, Hadinnapola C, Nikolic I, Wharton J, Guo J, Liley J, Haimel M, Bleda M, Southgate L, Machado RD, Martin JM, Treacy CM, Yates K, Daugherty LC, Shamardina O, Whitehorn D, Holden S, Bogaard HJ, Church C, Coghlan G, Condliffe R, Corris PA, Danesino C, Eyries M, Gall H, Ghio S, Ghofrani HA, Gibbs JSR, Girerd B, Houweling AC, Howard L, Humbert M, Kiely DG, Kovacs G, Lawrie A, MacKenzie Ross RV,

Moledina S, Montani D, Olschewski A, Olschewski H, Ouwehand WH, Peacock AJ, Pepke-Zaba J, Prokopenko I, Rhodes CJ, Scelsi L, Seeger W, Soubrier F, Suntharalingam J, Toshner MR, Trembath RC, Vonk Noordegraaf A, Wort SJ, Wilkins MR, Yu PB, Li W, Graf S, Upton PD, Morrell NW. Characterization of GDF2 Mutations and Levels of BMP9 and BMP10 in Pulmonary Arterial Hypertension. *Am J Respir Crit Care Med* 2019.

14. Eyries M, Montani D, Nadaud S, Girerd B, Levy M, Bourdin A, Tresorier R, Chaouat A, Cottin V, Sanfiorenzo C, Prevot G, Reynaud-Gaubert M, Dromer C, Houeijeh A, Nguyen K, Coulet F, Bonnet D, Humbert M, Soubrier F. Widening the landscape of heritable pulmonary hypertension mutations in paediatric and adult cases. *Eur Respir J* 2019; 53.
15. Wang XJ, Lian TY, Jiang X, Liu SF, Li SQ, Jiang R, Wu WH, Ye J, Cheng CY, Du Y, Xu XQ, Wu Y, Peng FH, Sun K, Mao YM, Yu H, Liang C, Shyy JY, Zhang SY, Zhang X, Jing ZC. Germline BMP9 mutation causes idiopathic pulmonary arterial hypertension. *Eur Respir J* 2019; 53.
16. Nikolic I, Yung LM, Yang P, Malhotra R, Paskin-Flerlage SD, Dinter T, Bocobo GA, Tumelty KE, Faugno AJ, Troncone L, McNeil ME, Huang X, Coser KR, Lai CSC, Upton PD, Goumans MJ, Zamanian RT, Elliott CG, Lee A, Zheng W, Berasi SP, Huard C, Morrell NW, Chung RT, Channick RW, Roberts KE, Yu PB. Bone Morphogenetic Protein 9 Is a Mechanistic Biomarker of Portopulmonary Hypertension. *Am J Respir Crit Care Med* 2019; 199: 891-902.
17. Owen NE, Alexander GJ, Sen S, Bunclark K, Polwarth G, Pepke-Zaba J, Davenport AP, Morrell NW, Upton PD. Reduced circulating BMP10 and BMP9 and elevated endoglin are associated with disease severity, decompensation and pulmonary vascular syndromes in patients with cirrhosis. *EBioMedicine* 2020; 56: 102794.

18. Li W, Long L, Hoenderdos K, Upton P, Yang X, Condliffe A, Chilvers E, Morrell N. S2 Vascular Quiescence Factor BMP9 is Regulated by Inflammation and Neutrophil Activation. *Thorax* 2015; 70: A5-A5.

19. Li W, Long L, Yang X, King R, Southwood M, Tong Z, Caruso P, Upton P, Salmon R, Condliffe A, Nourshargh S, Chilvers E, Morrell N. S39 Endogenous circulating BMP9 maintains endothelial barrier function. *Thorax* 2018; 73: A24-A24.

20. Li W, Long, L, Yang, X, King, R, Southwood, M, Jiang, H, Chilvers, ER, Nourshargh, S, Morrell, NW. Endogenous Circulating BMP9 Protects Lung Endothelial Barrier Function and Is Down-Regulated During LPS-Induced Inflammation. *Am J Respir Crit Care Med* 2018; 197, ATS2018 A97. Re-defining ALI pathogenesis: A2470.

21. Dolinay T, Kim YS, Howrylak J, Hunninghake GM, An CH, Fredenburgh L, Massaro AF, Rogers A, Gazourian L, Nakahira K, Haspel JA, Landazury R, Eppanapally S, Christie JD, Meyer NJ, Ware LB, Christiani DC, Ryter SW, Baron RM, Choi AM. Inflammasome-regulated cytokines are critical mediators of acute lung injury. *Am J Respir Crit Care Med* 2012; 185: 1225-1234.

22. Sun X, Icli B, Wara AK, Belkin N, He S, Kobzik L, Hunninghake GM, Vera MP, Registry M, Blackwell TS, Baron RM, Feinberg MW. MicroRNA-181b regulates NF-kappaB-mediated vascular inflammation. *J Clin Invest* 2012; 122: 1973-1990.

23. Malhotra R, Paskin-Flerlage S, Zamanian RT, Zimmerman P, Schmidt JW, Deng DY, Southwood M, Spencer R, Lai CS, Parker W, Channick RN, Morrell NW, Elliott CG, Yu PB. Circulating angiogenic modulatory factors predict survival and functional class in pulmonary arterial hypertension. *Pulmonary circulation* 2013; 3: 369-380.

24. Jiang H, Salmon RM, Upton PD, Wei Z, Lawera A, Davenport AP, Morrell NW, Li W. The Prodomain-bound Form of Bone Morphogenetic Protein 10 Is Biologically Active on Endothelial Cells. *J Biol Chem* 2016; 291: 2954-2966.

25. Salmon RM, Guo J, Wood JH, Tong Z, Beech JS, Lawera A, Yu M, Grainger DJ, Reckless J, Morrell NW, Li W. Molecular basis of ALK1-mediated signalling by BMP9/BMP10 and their prodomain-bound forms. *Nat Commun* 2020; 11: 1621.

26. van Baardewijk LJ, van der Ende J, Lissenberg-Thunnissen S, Romijn LM, Hawinkels LJ, Sier CF, Schipper IB. Circulating bone morphogenetic protein levels and delayed fracture healing. *Int Orthop* 2013; 37: 523-527.

27. Matute-Bello G, Downey G, Moore BB, Groshong SD, Matthay MA, Slutsky AS, Kuebler WM, Acute Lung Injury in Animals Study G. An official American Thoracic Society workshop report: features and measurements of experimental acute lung injury in animals. *Am J Respir Cell Mol Biol* 2011; 44: 725-738.

28. Andriopoulos B, Jr., Corradini E, Xia Y, Faasse SA, Chen S, Grgurevic L, Knutson MD, Pietrangelo A, Vukicevic S, Lin HY, Babitt JL. BMP6 is a key endogenous regulator of hepcidin expression and iron metabolism. *Nat Genet* 2009; 41: 482-487.

29. Hoenderdos K, Lodge KM, Hirst RA, Chen C, Palazzo SG, Emerenciana A, Summers C, Angyal A, Porter L, Juss JK, O'Callaghan C, Chilvers ER, Condliffe AM. Hypoxia upregulates neutrophil degranulation and potential for tissue injury. *Thorax* 2016; 71: 1030-1038.

30. Janciauskiene SM, Bals R, Koczulla R, Vogelmeier C, Kohnlein T, Welte T. The discovery of alpha1-antitrypsin and its role in health and disease. *Respir Med* 2011; 105: 1129-1139.

31. Gettins PG, Olson ST. Inhibitory serpins. New insights into their folding, polymerization, regulation and clearance. *Biochem J* 2016; 473: 2273-2293.

32. Chollet-Martin S, Montravers P, Gibert C, Elbim C, Desmonts JM, Fagon JY, Gougerot-Pocidalo MA. Subpopulation of hyperresponsive polymorphonuclear neutrophils in patients with adult respiratory distress syndrome. Role of cytokine production. *Am Rev Respir Dis* 1992; 146: 990-996.

33. Jimeno A, Posner MR, Wirth LJ, Saba NF, Cohen RB, Popa EC, Argiris A, Grossmann KF, Sukari A, Wilson D, Zhang X, Sun J, Glasser C, Attie KM, Sherman ML, Pandya SS, Weiss J. A phase 2 study of dalantercept, an activin receptor-like kinase-1 ligand trap, in patients with recurrent or metastatic squamous cell carcinoma of the head and neck. *Cancer* 2016; 122: 3641-3649.

34. Bendell JC, Gordon MS, Hurwitz HI, Jones SF, Mendelson DS, Blobe GC, Agarwal N, Condon CH, Wilson D, Pearsall AE, Yang Y, McClure T, Attie KM, Sherman ML, Sharma S. Safety, pharmacokinetics, pharmacodynamics, and antitumor activity of dalantercept, an activin receptor-like kinase-1 ligand trap, in patients with advanced cancer. *Clin Cancer Res* 2014; 20: 480-489.

35. Burton VJ, Ciuclan LI, Holmes AM, Rodman DM, Walker C, Budd DC. Bone morphogenetic protein receptor II regulates pulmonary artery endothelial cell barrier function. *Blood* 2011; 117: 333-341.

36. Bautch VL. Bone morphogenetic protein and blood vessels: new insights into endothelial cell junction regulation. *Curr Opin Hematol* 2019; 26: 154-160.

37. Benn A, Bredow C, Casanova I, Vukicevic S, Knaus P. VE-cadherin facilitates BMP-induced endothelial cell permeability and signaling. *J Cell Sci* 2016; 129: 206-218.

38. Hussein KA, Choksi K, Akeel S, Ahmad S, Megyerdi S, El-Sherbiny M, Nawaz M, Abu El-Asrar A, Al-Shabrawey M. Bone morphogenetic protein 2: a potential new player in the pathogenesis of diabetic retinopathy. *Exp Eye Res* 2014; 125: 79-88.

39. Helbing T, Wiltgen G, Hornstein A, Brauers EZ, Arnold L, Bauer A, Esser JS, Diehl P, Grundmann S, Fink K, Patterson C, Bode C, Moser M. Bone Morphogenetic Protein-Modulator BMPER Regulates Endothelial Barrier Function. *Inflammation* 2017; 40: 442-453.

40. Li Z, Wang J, Wang Y, Jiang H, Xu X, Zhang C, Li D, Xu C, Zhang K, Qi Y, Gong X, Tang C, Zhong N, Lu W. Bone morphogenetic protein 4 inhibits liposaccharide-induced inflammation in the airway. *Eur J Immunol* 2014; 44: 3283-3294.

41. Wang K, Gong J, Pei L, Shan S, Tan W. The effect of rhBMP-2 on pulmonary arterioles remodeling in endotoxin-induced acute lung injury in rats. *Clin Exp Med* 2013; 13: 187-192.

42. Young K, Conley B, Romero D, Tweedie E, O'Neill C, Pinz I, Brogan L, Lindner V, Liaw L, Vary CP. BMP9 regulates endoglin-dependent chemokine responses in endothelial cells. *Blood* 2012; 120: 4263-4273.

43. Hiepen C, Jatzlau J, Hildebrandt S, Kampfrath B, Goktas M, Murgai A, Cuellar Camacho JL, Haag R, Ruppert C, Sengle G, Cavalcanti-Adam EA, Blank KG, Knaus P. BMPR2 acts as a gatekeeper to protect endothelial cells from increased TGFbeta responses and altered cell mechanics. *PLoS Biol* 2019; 17: e3000557.

44. Bates DO. Vascular endothelial growth factors and vascular permeability. *Cardiovasc Res* 2010; 87: 262-271.

45. Ruiz S, Zhao H, Chandakkar P, Chatterjee PK, Papoin J, Blanc L, Metz CN, Campagne F, Marambaud P. A mouse model of hereditary hemorrhagic telangiectasia generated by transmammary-delivered immunoblocking of BMP9 and BMP10. *Sci Rep* 2016; 5: 37366.

46. Bai C, Fukuda N, Song Y, Ma T, Matthay MA, Verkman AS. Lung fluid transport in aquaporin-1 and aquaporin-4 knockout mice. *J Clin Invest* 1999; 103: 555-561.

47. King LS, Nielsen S, Agre P, Brown RH. Decreased pulmonary vascular permeability in aquaporin-1-null humans. *Proc Natl Acad Sci U S A* 2002; 99: 1059-1063.

48. Lai KN, Leung JC, Metz CN, Lai FM, Bucala R, Lan HY. Role for macrophage migration inhibitory factor in acute respiratory distress syndrome. *J Pathol* 2003; 199: 496-508.

49. Breitkopf-Heinlein K, Meyer C, Konig C, Gaitantzi H, Addante A, Thomas M, Wiercinska E, Cai C, Li Q, Wan F, Hellerbrand C, Valous NA, Hahnel M, Ehlting C, Bode JG, Muller-Bohl S, Klingmuller U, Altenoder J, Ilkavets I, Goumans MJ, Hawinkels LJ, Lee SJ, Wieland M, Mogler C, Ebert MP, Herrera B, Augustin H, Sanchez A, Dooley S, Ten Dijke P. BMP-9 interferes with liver regeneration and promotes liver fibrosis. *Gut* 2017; 66: 939-954.

50. Talati M, Mutlak, H, Lane, KB, Han, W, Hemnes, A, Mutlak, O, Blackwell, T, Zaynagetdinov, R, Blackwell, TS and West, J. NF-κB Activation Exacerbates, but Is not Required for Murine Bmpr2-Related Pulmonary Hypertension. *Diseases* 2014; 2.

51. Appleby SL, Mitrofan CG, Crosby A, Hoenderdos K, Lodge K, Upton PD, Yates CM, Nash GB, Chilvers ER, Morrell NW. Bone Morphogenetic Protein 9 Enhances Lipopolysaccharide-Induced Leukocyte Recruitment to the Vascular Endothelium. *J Immunol* 2016; 197: 3302-3314.

52. Mitrofan CG, Appleby SL, Nash GB, Mallat Z, Chilvers ER, Upton PD, Morrell NW. Bone morphogenetic protein 9 (BMP9) and BMP10 enhance tumor necrosis factor-alpha-induced monocyte recruitment to the vascular endothelium mainly via activin receptor-like kinase 2. *J Biol Chem* 2017; 292: 13714-13726.

53. Goldenberg NM, Steinberg BE, Slutsky AS, Lee WL. Broken barriers: a new take on sepsis pathogenesis. *Sci Transl Med* 2011; 3: 88ps25.

54. London NR, Zhu W, Bozza FA, Smith MC, Greif DM, Sorensen LK, Chen L, Kaminoh Y, Chan AC, Passi SF, Day CW, Barnard DL, Zimmerman GA, Krasnow MA, Li DY. Targeting Robo4-dependent Slit signaling to survive the cytokine storm in sepsis and influenza. *Sci Transl Med* 2010; 2: 23ra19.

55. Carvalho BS, Irizarry RA. A framework for oligonucleotide microarray preprocessing. *Bioinformatics* 2010; 26: 2363-2367.

56. Irizarry RA, Hobbs B, Collin F, Beazer-Barclay YD, Antonellis KJ, Scherf U, Speed TP. Exploration, normalization, and summaries of high density oligonucleotide array probe level data. *Biostatistics* 2003; 4: 249-264.

57. Ritchie ME, Phipson B, Wu D, Hu Y, Law CW, Shi W, Smyth GK. limma powers differential expression analyses for RNA-sequencing and microarray studies. *Nucleic Acids Res* 2015; 43: e47.

58. Benjamini Y, Hochberg Y. Controlling the false discovery rate - a practical and powerful approach to multiple testing. *Journal of the Royal Statistical Society Series B - Methodological* 1995; 57: 289-300.

FIGURE LEGENDS:

Figure 1. Neutralizing endogenous BMP9 results in lung vascular leak and neutrophil extravasation. (A) A schematic diagram indicating the treatment regimen. (B) Inhibiting endogenous BMP9 activity leads to lung vascular leak. Left, representative images of the lungs, showing the Evans Blue (EB)-stained lungs from LPS and anti-BMP9 treated animals. Right, quantification of EB content in the lungs. N=6 per group. (C&D) Anti-BMP9 treatment leads to an increase in the perivascular adventitial area, similar to LPS-treatment (black arrows). (C) Representative pictures of H&E stained lung section. Scale bars = 100 μM. (D) Adventitial area in 20 random high-power field (HPF), with its correlation to the EB content in the lung shown on the right; Spearman's correlation test. (E) Anti-BMP9 treatment increases alveolar neutrophil counts, revealed by myeloperoxidase staining. Scale bars = 50 μM. The counts were the mean of six random HPF per animal. (F) BMP9 activity in plasma measured by *ID1*-gene induction in hPAECs. Serum-starved hPAECs were treated with 1% plasma samples for 1 hour before cells were harvested for RT-qPCR analysis of *ID1* gene induction. The operator was blinded to the treatment samples. For all panels, data are shown as means ± SEM. Two-tailed, Mann-Whitney test, LPS treatment comparing with PBS-treated controls, and anti-BMP9 comparing with IgG-treated controls. * , $P < 0.05$; ** , $P < 0.01$; *** $P < 0.001$; n.s., not significant.

Figure 2. BMP9 signaling regulates genes involved in endothelial cell integrity. (A) A volcano plot of microarray transcriptional analysis of BMP9 regulated genes. Serum-starved hPAECs were treated with 0.4 ng/ml (GF-domain concentration) pro-BMP9 for 5 hours before cells were harvested for microarray analysis using Human Gene 2.1 ST array. Four independent hPAEC lines were used. Data were processed using package Oligo in R (55), normalized using Robust Multichip Analysis (RMA)(56), and comparisons were performed using the limma package (57). Resulting P-values were corrected for multiple testing using False Discovery Rate

(FDR)(58). Hits with adjusted P-values of less than 0.05 are shown in red. (B) Validation of microarray results using RT-qPCR. BMP9 signaling regulates mRNA expression of *AQP1* (Aquaporin1), *KDR* (VEGFR2) and *TEK* (Tie2) in hPAECs. N=5. (C) Changes of gene expression in hPAECs after inhibition of BMP9 activity in FBS with a neutralizing anti-BMP9 antibody. PAECs were grown in endothelial basal medium with 2% FBS, treated with IgG control or anti-BMP9 antibody (both at 20 μg/ml) for 3 hours (for *TEK*) or 5 hours (for *AQP1* and *KDR*) before cells were harvested for RNA extraction and qPCR analysis. N=5. (D) BMP9-treatment suppresses VEGFR2 total proteins. Serum-starved hPAECs were treated with pro-BMP9 (0.4 ng/ml GF-domain concentration) for 5 hours, N=6. Three independent treatments were run on the same western blot and shown. Quantification was performed using ImageJ and loading corrected by β actin controls. Changes upon BMP9-treatment relative to PBS controls were calculated and shown as means ± SEM. Two-tailed Wilcoxon test. *, $P < 0.05$. (E) BMP9 regulates *AQP1, KDR* and *TEK* expressions in human pulmonary microvascular endothelial cells (hPMECs). (F) In hPMECs, anti-BMP9 treatment leads to enhanced apoptosis measured using Caspase 3/7 Glo assay. (G) Anti-BMP9 treatment in hPMECs causes enhanced monolayer permeability measured by HRP-transwell assay as described previously(8). For B, C and E-G, means ± SEM are shown, two-tailed, Mann-Whitney test, *, $P < 0.05$; **, $P < 0.01$.

Figure 3. BMP9 prevents vascular leak and lung injury in inhaled LPS-challenged mice involves *TEK* and *KDR*. (A) Representative images of H&E-stained lung tissues. Mice were challenged intranasally with LPS (at 20 μg/mouse) for 24 hours before lungs were harvested for immunohistological examination. (B) BMP9 prevented vascular leak measured by EB retained in the lungs. (C) BMP9 protected ALI induced by inhaled LPS. Lung injury scores were based on 20 HPF per animal as per protocol from the American Thoracic Society Workshop report (27)(More details can be found in the **Extended Methods** in the online supplement). (D)

Administration of BMP9 prevented the extravasation of neutrophils into the alveolar space. Neutrophils were counted from the H&E-stained slides based on the shape of the cells and nuclei. (E) Administration of BMP9 prevented the increase of plasma elastase after inhaled LPS-challenge. (F-I) Lung mRNA expression measured by qPCR. *RPL32* was used as the house-keeping gene. The operator was blinded to the treatment in this experiment. For all panels, means ± SEM are shown, one-way ANOVA, Tukey's post test. *, P < 0.05; **, P < 0.01; ***, P < 0.001; ****, P < 0.0001.

Figure 4. Endogenous BMP9 is reduced in endotoxemia mice and sepsis patients *(A) Circulating BMP9 levels are significantly reduced in murine endotoxemia model*. Mice were treated with 2 mg/kg LPS intraperitoneally for 18 hours before plasma were taken for BMP9 measurement. N=12, Data are shown as means ± SEM. Two-tailed, unpaired t-test, ****, P < 0.0001. *(B) Dynamic changes in circulating BMP9 after LPS-induced inflammation.* Mice were treated with 2 mg/kg LPS intraperitoneally and sacrificed at 0, 0.75, 3, 6, 18 and 24 hours. N=6 per group. Three animals were treated with PBS at each time point and used as controls. Concentrations of BMP9 in plasma were measured by ELISA, normalized to controls. (*C-E) Dynamic changes of liver mRNA expression relative to controls after LPS-challenge.* Data were analyzed using the ΔΔCt method, using RPL32 as the house keeping gene. *(F) Changes in plasma elastase (red line) and AAT (black line) protein levels relative to controls during endotoxemia.* The actual control value for AAT is 3.44 ± 0.09 mg/ml, for elastase is 128.6 ± 26.8 ng/ml. (G) *Plasma BMP9 concentrations from SIRS and sepsis patients are significantly lower than those from healthy controls*. In measurement B to G, means ± SEM are shown, one-way ANOVA, Dunnett's post test against controls, *, P < 0.05; **, P < 0.01; *** P < 0.001; ****, P < 0.0001.

Figure 5. BMP9 is a substrate for neutrophil elastase. (*A) BMP9 is a direct substrate of elastase.* Purified pro-BMP9 was incubated with recombinant human neutrophil elastase (HNE) or trypsin at indicated concentration (% w/w) in PBS overnight and the mixture was fractionated by SDS-PAGE under reducing conditions and visualized by Coomassie Blue Staining. P: prodomain. (B) *A schematic diagram illustrating the generation of supernatants from activated neutrophils*. Neutrophils were isolated from the peripheral blood of healthy volunteers, incubated under hypoxia for 4 hours before priming with GM-CSF and activation with fMLP as described previously (29). *(C&D) Neutrophil elastase is the major protease cleaving pro-BMP9 in the activated neutrophil supernatant*. Pro-BMP9 was incubated with the supernatant from activated neutrophils in the presence or absence of a panel of protease inhibitors overnight and the mixture fractionated by SDS-PAGE under reducing conditions and visualized by Coomassie Blue Staining. A representative gel from 4 independent experiments is shown in (C, two parts of the same gels are shown) and the quantification of BMP9 bands from 4 experiments in (D). Means ± SEM are shown, two-tailed, Mann-Whitney test. *, $P < 0.05$; ns, not significant.

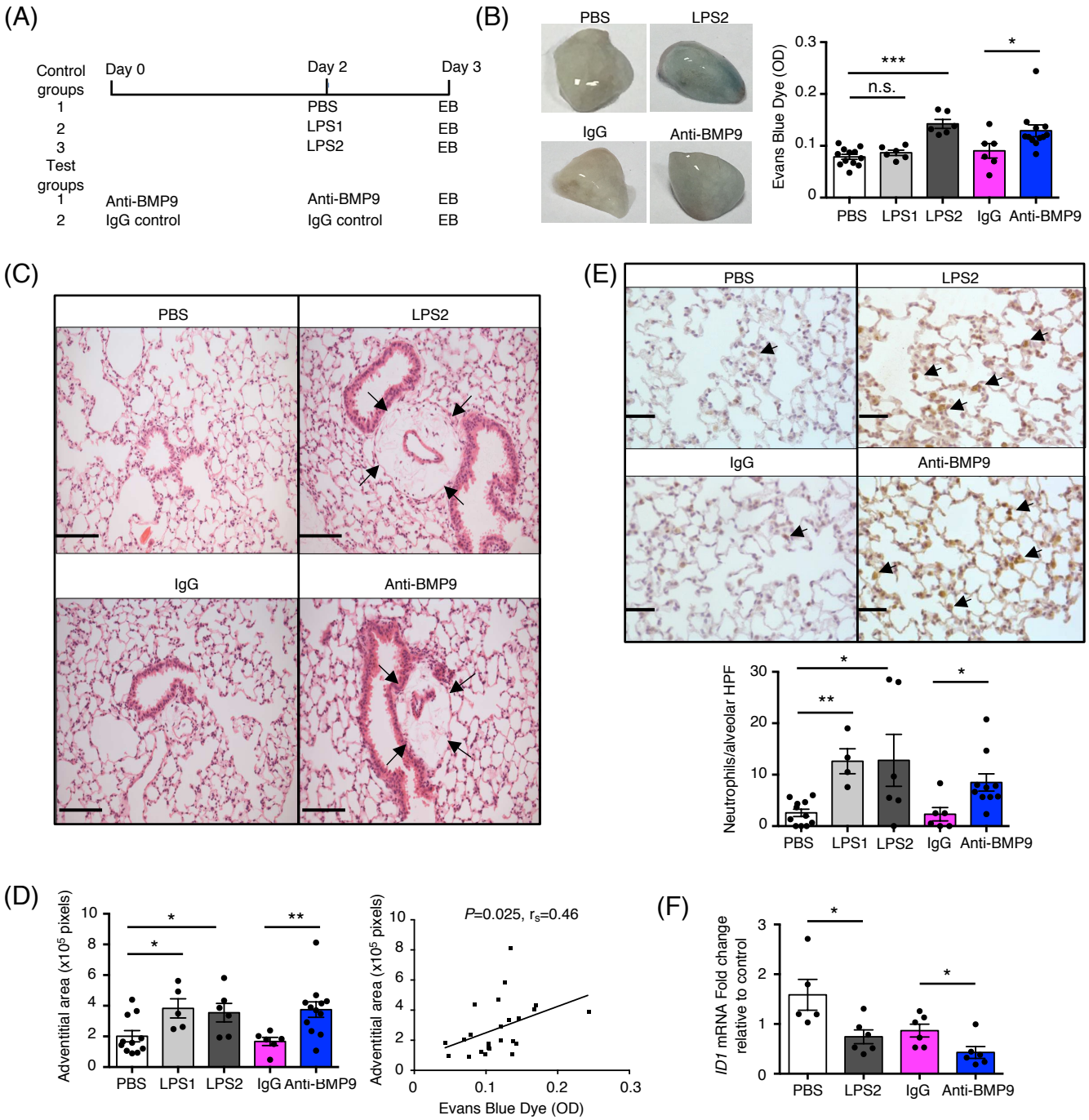
(A)
Control groups
Day 0
Day 2
Day 3
1
PBS
EB
2
LPS1
EB
3
LPS2
EB
Test groups
1
Anti-BMP9
Anti-BMP9
EB
2
IgG control
IgG control
EB
(B)
PBS
LPS2
IgG
Anti-BMP9
Evans Blue Dye (OD)
0.3
0.2
0.1
0
***
n.s.
*
PBS
LPS1
LPS2
IgG
Anti-BMP9
(C)
PBS
LPS2
IgG
Anti-BMP9
(E)
PBS
LPS2
IgG
Anti-BMP9
Neutrophils/alveolar HPF
30
20
10
0
*
**
*
PBS
LPS1
LPS2
IgG
Anti-BMP9
(D)
Adventitial area (x10^5 pixels)
10
8
6
4
2
0
*
*
**
PBS
LPS1
LPS2
IgG
Anti-BMP9
Adventitial area (x10^5 pixels)
P=0.025, r_s=0.46
0
0.1
0.2
0.3
Evans Blue Dye (OD)
(F)
ID1 mRNA Fold change relative to control
3
2
1
0
*
*
PBS
LPS2
IgG
Anti-BMP9

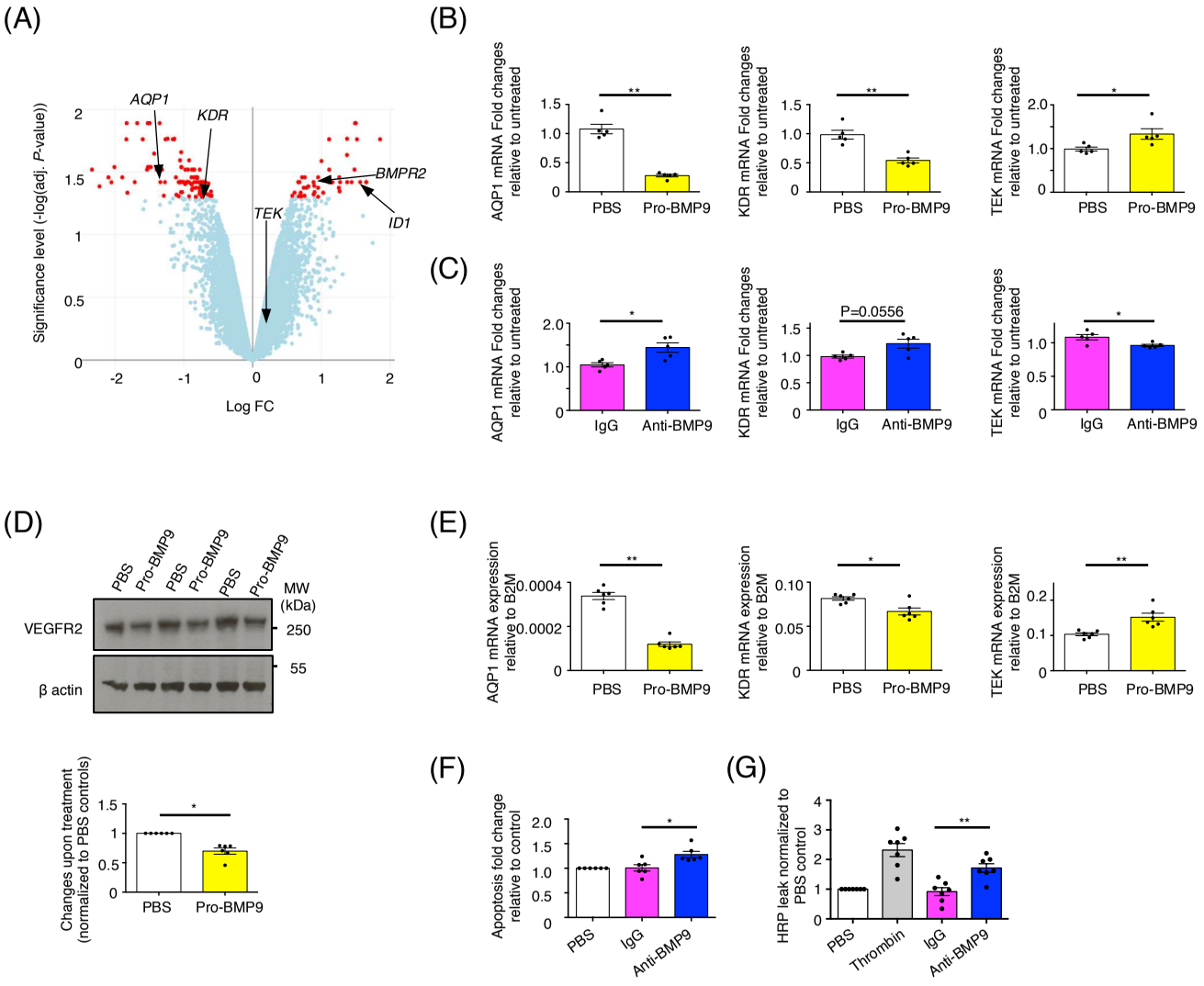
(A)
AQP1
KDR
BMPR2
TEK
ID1
Significance level (-log(adj. P-value))
Log FC
(B)
AQP1 mRNA Fold changes relative to untreated
KDR mRNA Fold changes relative to untreated
TEK mRNA Fold changes relative to untreated
PBS
Pro-BMP9
(C)
IgG
Anti-BMP9
P=0.0556
(D)
VEGFR2
β actin
MW (kDa)
250
55
Changes upon treatment (normalized to PBS controls)
(E)
AQP1 mRNA expression relative to B2M
KDR mRNA expression relative to B2M
TEK mRNA expression relative to B2M
(F)
Apoptosis fold change relative to control
(G)
HRP leak normalized to PBS control
Thrombin

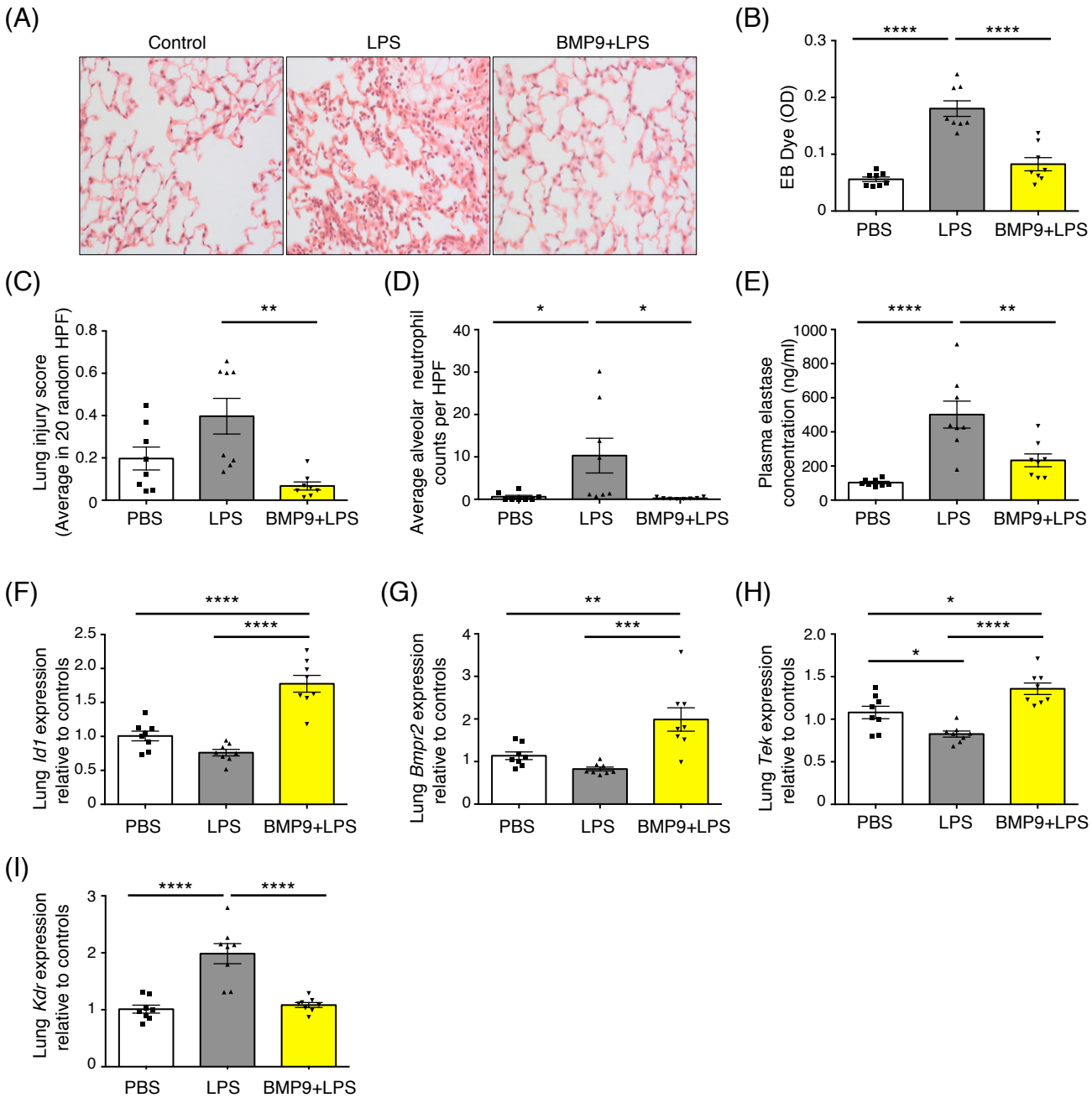
(A)
Control
LPS
BMP9+LPS
(B)
EB Dye (OD)
PBS
LPS
BMP9+LPS
(C)
Lung injury score (Average in 20 random HPF)
(D)
Average alveolar neutrophil counts per HPF
(E)
Plasma elastase concentration (ng/ml)
(F)
Lung Id1 expression relative to controls
(G)
Lung Bmpr2 expression relative to controls
(H)
Lung Tek expression relative to controls
(I)
Lung Kdr expression relative to controls

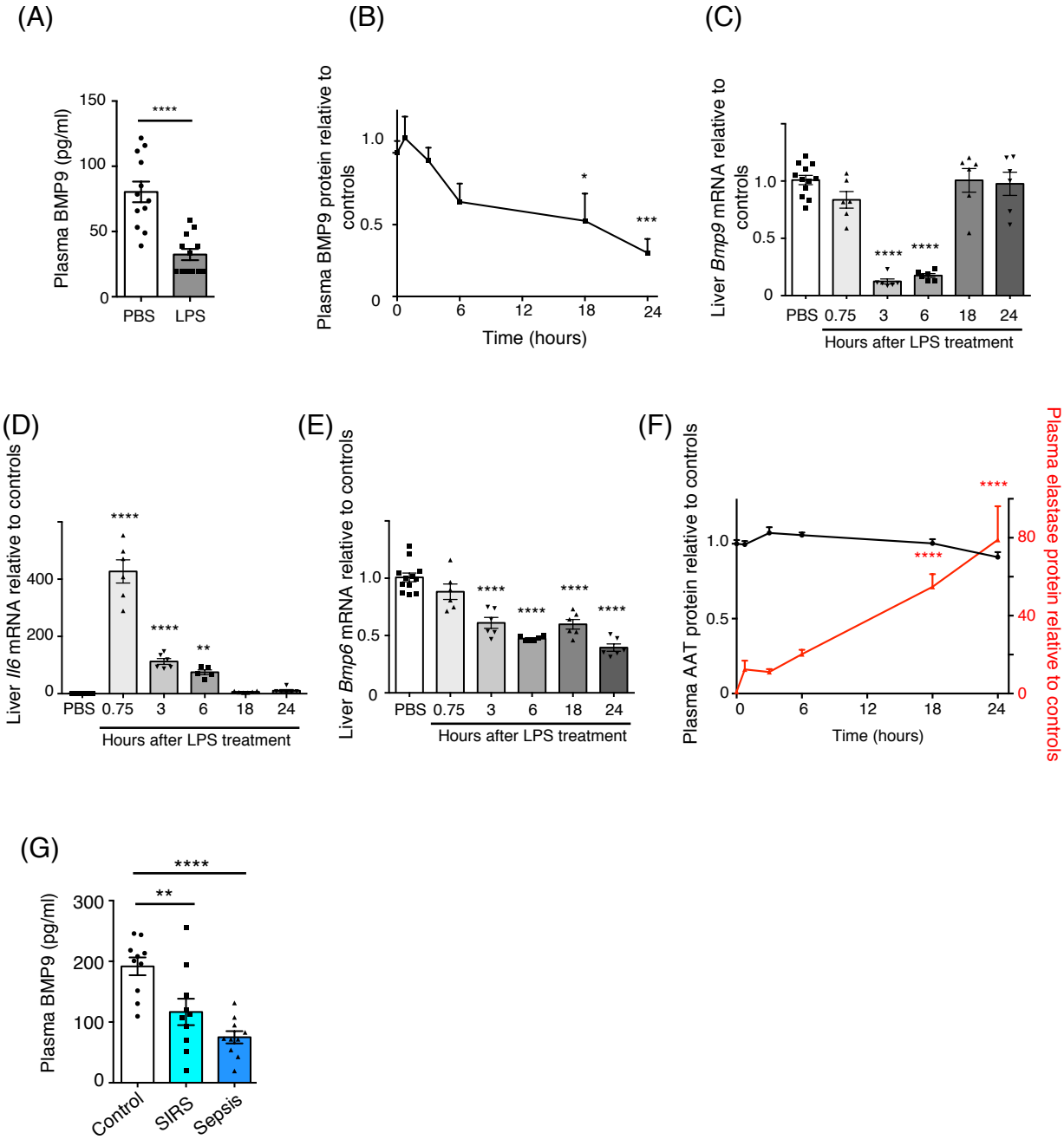
(A)
Plasma BMP9 (pg/ml)
150
100
50
0
****
PBS
LPS
(B)
Plasma BMP9 protein relative to controls
1.0
0.5
0
*
***
0
6
12
18
24
Time (hours)
(C)
Liver Bmp9 mRNA relative to controls
1.0
0.5
0
****
****
PBS
0.75
3
6
18
24
Hours after LPS treatment
(D)
Liver Il6 mRNA relative to controls
400
200
0
****
****
**
PBS
0.75
3
6
18
24
Hours after LPS treatment
(E)
Liver Bmp6 mRNA relative to controls
1.0
0.5
0
****
****
****
****
PBS
0.75
3
6
18
24
Hours after LPS treatment
(F)
Plasma AAT protein relative to controls
1.0
0.5
0
****
****
0
6
12
18
24
Time (hours)
Plasma elastase protein relative to controls
80
40
0
(G)
Plasma BMP9 (pg/ml)
300
200
100
0
****
**
Control
SIRS
Sepsis

(A)

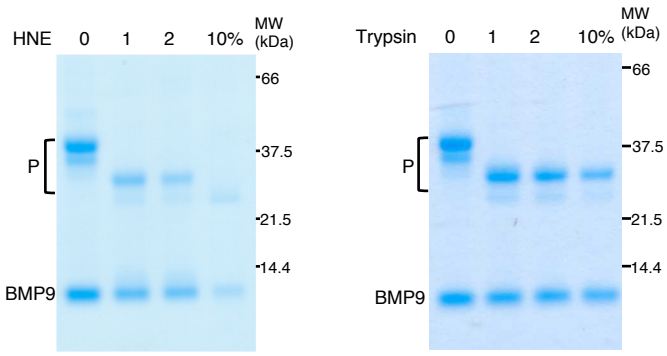
HNE
0
1
2
10%
MW (kDa)
66
37.5
21.5
14.4
P
BMP9
Trypsin
0
1
2
10%
MW (kDa)
66
37.5
21.5
14.4
P
BMP9

(B)

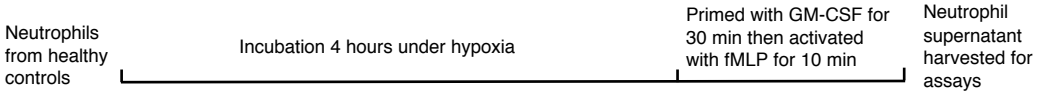
Neutrophils from healthy controls
Incubation 4 hours under hypoxia
Primed with GM-CSF for 30 min then activated with fMLP for 10 min
Neutrophil supernatant harvested for assays

(C)

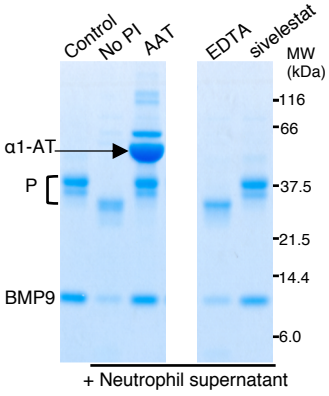
Control
No PI
AAT
EDTA
sivelestat
MW (kDa)
116
66
37.5
21.5
14.4
6.0
α1-AT
P
BMP9
+ Neutrophil supernatant

(D)

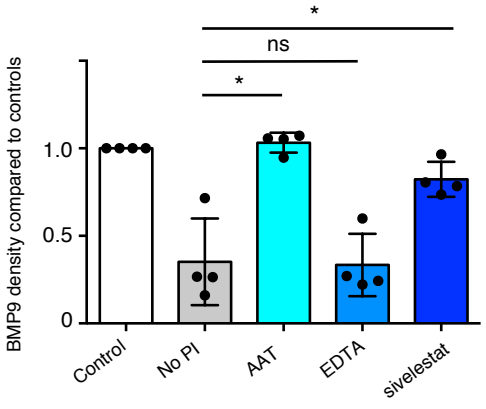
*
ns
*
BMP9 density compared to controls
1.0
0.5
0
Control
No PI
AAT
EDTA
sivelestat

Endogenous BMP9 protects pulmonary vascular endothelium and is down-regulated during inflammation

Wei Li[1,*,$], Lu Long[1], Xudong Yang[1], Zhen Tong[1], Mark Southwood[1], Ross King[2], Paola Caruso[1], Paul D Upton[1], Peiran Yang[3], Geoffrey A Bocobo[3], Ivana Nikolic[4], Angelica Higuera[5], Richard M Salmon[1], He Jiang[1], Katharine M Lodge[6], Kim Hoenderdos[1], Rebecca M Baron[5], Paul B Yu[3], Alison M Condliffe[7], Charlotte Summers[1], Sussan Nourshargh[2], Edwin R Chilvers[6], Nicholas W Morrell[1,*,$]

ONLINE DATA SUPPLEMENT:

Expanded materials and methods

Expanded materials and methods

Materials:

Male C57BL/6 mice (12 weeks old, ~25-30g) were purchased from Charles River and used for all *in vivo* studies. Mouse elastase ELISA kit was purchased from Cloud-Clone Corp (Cat No. SEA181Mu). Mouse α1-antitrypsin ELISA kit was purchased from GenWay Biotech Inc (Cat No. GWB-DB430D). Both mouse monoclonal (Cat No. MAB3209) and biotinylated goat polyclonal (Cat No. BAF3209) anti-BMP9 antibodies, and IgG2B (MAB004) were purchased from R&D Systems. Endothelial cell basal media (EBM-2) were purchased from Lonza or PromoCell; and supplemented with a Bullet kit (Lonza) to obtain endothelial growth medium (EGM-2). All plasmid and RNA purification kits were purchased from Qiagen. LPS was from Sigma Aldrich (Cat No. L2630). Total blood count was carried out using the scil Vet ABC ™Hematology Analyzer (Woodley Equipment Company LTD). Recombinant human neutrophil elastase was purchased from AppliChem.

Expression and purification of pro-BMP9. Transfection and purification of pro-BMP9, which is the circulating form and consists of the prodomain non-covalently complexed with the growth factor domain (GF-domain), were achieved following previously described protocols (1, 2).

Observation and quantification of systemic microvascular leakage by intravital confocal microscopy. Systemic microvascular leakage *in vivo* was assessed by tracking the tissue infiltration of intravenously injected fluorescent Dextran in mouse cremaster muscles, as observed by intravital confocal microscopy and previously detailed (3). Briefly, male C57BL/6J mice (aged 6-8 weeks) were anaesthetized by inhalation of isoflurane (3% isoflurane in air) and received an intrascrotal injection of a non-blocking anti-CD31 mAb conjugated with Alexa

Fluor 647 (C390; eBioscience; 4 μg/mouse), a procedure that we have previously developed for efficient *in vivo* labelling of vascular endothelial cells (3, 4). Mice were allowed to recover for 2 hours prior to receiving an intraperitoneal injection of ketamine (100 mg/kg) and xylazine (10 mg/kg) to induce terminal anaesthesia, and subsequently surgical exteriorization of the cremaster muscle, as previously detailed (4). Tissues were observed using a Leica SP5 confocal microscope incorporating a 20x water-dipping objective (NA 1.0) and postcapillary venules of 20-40 μm diameter were selected for *in vivo* analysis of microvascular leakage. Images were acquired every minute with sequential scanning of different channels at a resolution of 1,024 x 512 pixels in the xy planes and 0.7 μm steps in the z plane. After 5 minutes of baseline recording, 40 mg/kg TRITC-Dextran (molecular weight 65-85 kDa, Sigma-Aldrich) was injected intravenously and allowed to circulate for a further 3 minutes. Following this, mice received i.v. anti-BMP9 or IgG isotype control (both at 5 mg/kg) via the tail vein and recordings were made for up to 1 hour. As a positive control, 100 μM histamine was prepared in warm Tyrode's solution and superfused over the cremaster muscle (2.25 μmoles) to elicit microvascular leakage. Confocal image sequences of microvascular leakage were analyzed with IMARIS 4D modeling software (Bitplane) and temporal accumulation of TRITC-Dextran in the interstitial tissue was quantified by mean fluorescence intensity (MFI) of perivascular tissues (within 50 μm of the venular wall) every minute.

***Neutrophil elastase cleavage assay*.** Neutrophils were isolated from peripheral blood and activated *in vitro* under hypoxia as described previously(5). Five μg of recombinant pro-BMP9 was incubated at room temperature overnight, in a final volume of 20 μl in PBS, containing 5 μl of activated neutrophil supernatant (generated as described previously (5)) without or with protease inhibitors. The mixture was separated on a 12% SDS-PAGE (NuPAGE, Invitrogen)

under reducing conditions and visualized by Coomassie Blue staining. The band intensities of BMP9 GF-domain were quantified using Image J.

Murine endotoxemia studies. Mice were injected intraperitoneally with 2 mg/kg LPS or vehicle. After the length of time as specified in figure legends, mice were sacrificed using ketamine and xylazine. Bronchoalveolar lavage fluid (BALF) was collected by injecting and recovering 1 ml PBS via trachea. Blood for plasma preparation was taken via the inferior vena cava. Liver and right lung were snap frozen for RNA extraction while the left lung was inflated with a 1:1 mixture of saline and O.C.T. compound (Sakura, Zoeterwoude, Netherlands), fixed with 4% paraformaldehyde in PBS before dehydration and paraffin embedding for immunohistochemistry.

Measuring gene expression in mouse liver. Liver total mRNA was extracted using Qiagen miRNeasy Mini kit following manufacturer's instruction. After measuring the mRNA concentration on a Nanodrop Spectrometer, 1 ng was included in the reverse transcription reaction using High-Capacity cDNA Reverse Transcription Kit (Applied Biosystems) following the manufacturer's instruction. Quantitative PCR (qPCR) was carried out in 384 well plate on a Quantstudio 6™ Real-Time thermal cycler (Applied Biosystems) and the relative expression of target mRNA was normalized to Ribosomal Protein L32 (*Rpl32*) using the ΔΔCT method(6), expressed as the fold-changes relative to PBS treated controls. The following forward and reverse primers were used to amplify the corresponding mouse genes: α1-AT: 5' GGCCATACCCATGTCTATCC-3'; 5' TTCACCACTTTTCCCATGAA-3', *Bmp9*: 5'-ACAACGGACAAATCGTCTACG-3'; 5'- AGGATGTGCTTCTGAAAGGGG-3'. QuantiTect primers (Qiagen) were used for mouse *Bmp6* and *Il6*.

Haematoxylin and eosin (H&E) staining and lung injury scoring. Four μm mouse lung sections were H&E stained and examined by light microscopy. Lung injury was scored following the published guidelines (7). Briefly, 20 high power fields from each mouse H&E slides were scored 0-2 for the following 5 parameters: A. Neutrophils in the alveolar space, B. Neutrophils in the interstitial space, C. Hyaline membranes, D. Proteinaceous debris filling the airspaces, E. Alveolar septal thickening. ALI scores were then calculated using the following equation: Score = [(20 x A) + (14 x B) + (7 x C) + (7 x D) + (2 x E)]/(number of fields x 100). Mice neutrophils were immunostained using rabbit-polyclonal anti-myeloperoxidase (DakoCytomation, UK), labelled using immunoperoxidase (Vectastain Elite, Vector Laboratories) and 3,3′-DAB to create a brown coloured reaction product as previously described (8). All immune-histochemistry scorings were carried out in a blinded manner.

PAEC signaling assay for evaluating plasma BMP9 activity. Human PAECs were grown to ~80% confluence, serum-starved overnight in EGM-2 containing 0.1% FBS before treating with 1% mouse plasma. After 1 hour, cells were snap-frozen to stop the signaling and harvested for mRNA analysis. RNA extraction, reverse transcription and qPCR analysis were carried out as described above. The following primers were used for the qPCR reactions: human *ID1*: 5'-CTGCTCTACGACATGAACGGC-3', 5'-TGACGTGCTGGAGAATCTCCA-3'; human β2 microglobulin (*B2M*): 5'-CTCGCGCTACTCTCTCTTTCT-3', 5'-CATTCTCTGCTGGATGACGTG-3'.

***Pro-BMP9 signaling in hPAECs and microarray*.** For the microarray experiment, 4 different lines of hPAECs were serum-starved overnight in EGM-2 containing 0.1% FBS before being treated with pro-BMP9 (at 0.4 ng/ml of GF-domain concentration) for 5 hours. Cells were snap-frozen and harvested for mRNA extraction and microarray analysis. Microarray experiments were performed at Cambridge Genomic Services, using a human Gene 2.1 ST Array Plate

(Affymetrix, Wooburn Green, UK) in combination with WT PLUS amplification kit (Affymetrix) according to the manufacturer's instructions. Following data processing using package Oligo in R (9), normalization was carried out using Robust Multichip Analysis (RMA)(10), and comparisons were performed using the limma package (11). The results were corrected for multiple testing using False Discovery Rate (FDR)(12). Protein-protein interaction (PPI) and enriched pathway analysis were performed using STRING (13). Validation of the target genes identified by microarray were carried out by RT-qPCR. The following primers were used for the qPCR reactions: human *AQP1*: 5'TCTCAGGCATCACCTCCTCC-3', 5'CGAGTTCACACCATCAGCCA-3'; human *KDR*: 5'GATGCAGGAAACTACACGGTCA-3', 5'TCCATAGGCGAGATCAAGGCT-3'; human *TEK*: 5'GAAACATCCCTCACCTGCATTG-3', 5'TTTCGCCCATTCTCTGGTCA-3'. Microarray data have been deposited to Gene Expression Omnibus, with the accession number of GSE118353.

Anti-BMP9 treatment of hPAECs for qPCR. Human PAECs were cultured in EBM-2 containing 2% FBS for at least 20 hours before treatment with 20 μg/ml anti-BMP9 antibody (MAB3209, R&D systems) or 20 μg/ml IgG2B (MAB004, R&D systems) for 3 or 5 hours. Cells were snap-frozen to stop the signaling and harvested for mRNA analysis. RNA extraction, reverse transcription and qPCR analysis were carried out as described above.

Apoptosis assay. Apoptosis assay was performed using Caspase-Glo 3/7 Assay System (Promega, Cat. No. G8090). PMECs were seeded in triplicates at 10,000 cells per well in 96-well cell culture plates overnight in EGM-2 containing 10% FBS. On the following day, cells were incubated with 100 μl fresh endothelial basal medium (EBM-2) containing 2% FBS with different treatment reagents: anti-BMP9 antibody (at 100 μg/ml), IgG (at 100 μg/ml), or vehicle control (0.5%BSA in PBS). After 5 hours, cells were harvested by adding 100 μl substrate reagent to each well. The plates were protected from light by foil and mixed at 400 rpm for 20

min. 100 µl supernatant was transferred to a 96-well white wall plate and luminescence changes were recorded in a microplate luminometer.

Permeability assay. PMECs were seeded at 1 x 10^5 cells per trans-well insert (Costar) in EGM-2 with 10% FBS and incubated for 24 hours. On the next day, inserts were moved to a new chamber with 2 % FBS in EBM-2, and the upper chamber medium were changed to 2 % FBS in EBM-2 containing 20 nM HRP that was supplemented with anti-BMP9 antibody (at 100 µg/ml) or IgG (at 100 µg/ml), along with a positive control (0.2 Unit/ml Thrombin) and a negative control (an equal volume of medium). At 10 min, 15 µl medium from the lower chamber was collected and transferred to a 96 well plate. 150 µl buffer containing HRP substrate (o-phenylenediamine dihydrochloride) was added and the plate was read at 490 nm immediately.

siRNA knockdown and permeability assay. PMECs were seeded in six well plate (200k cells/well) and cultured for 24 hours in EGM-2 supplement with 5 % FCS before transfection. For siRNA transfection, cells were first incubated in Opti-MEM I for 1 hour and then transfected with 10 nM siBMPR2, siCP or the transfection reagent DharmaFECT1 alone (DH1) in Opti-MEM I for 4 hours. The transfection medium was replaced with full growth medium and cells were incubated for 24 hours before being seeded for functional assay. For permeability assay, transfected cells were seeded at 0.2 million per transwell insert (Costar) and incubated for 48 hours in EGM-2 supplement with 5 % FCS before treatment. On the day of assay, cell medium was changed to 0.1 % FCS basal medium and transfected cells were treated with or without 20 ng/ml pro-BMP9 for 30 min prior to LPS treatment (4 µg/ml) in the presence of 20 nM HRP as described above. Three samples were taken from the lower chamber at 45 min and transferred to 96 well plate for HRP activity reading as described above. Knockdown efficiency was confirmed by qPCR using transfected cells that harvested on the day of the permeability assay.

Anti-BMP9 treatment of hPAECs for VE-cadherin staining. PAECs were seeded at 110,000 cells/chamber onto collagen-coated BD FalconTM glass chamber slides (BD Biosciences, Oxford, UK) and cultured for 48 hours prior to the treatment with 100 μg/ml of anti-BMP9 or IgG for 15 minutes. After the treatment the chamber slides were washed with PBS, fixed with methanol and permeabilized with 0.5% Triton-X-100. Prior to staining cells were blocked with 0.5% BSA. After blocking, cells were incubated with a mouse anti-human-CD144 (BD Biosciences, Oxford, UK, cat.555661) followed by a goat anti-mouse Alexa-Fluor 488 secondary antibody (Life Technologies, Glasgow, UK). Nuclei were counterstained using DAPI (Vectashield, Peterborough, UK). Cells were viewed and photographed using a confocal microscope (Leica TCS SP5) and images captured using Leica LAS AF software. For the quantification, Fiji software (Fiji for Mac OS X, https://fiji.sc) was used. Fluorescence intensity was calculated as total pixel/area above a threshold value of 85-90 using a single threshold value for all samples within a same experiment. Fluorescence was calculated as mean of 4-12 for group in each experiment, normalized to the total cell number (DAPI positive cells) in each image. Final quantifications were obtained from three independent experiments.

Table E1. List of genes that are upregulated by pro-BMP9 following 5-hour treatment in PAECs. Microarray experiment is described in the Expanded Materials and Methods. Hits with adjusted P values less than 0.05 are shown.

Gene assignment	Gene name	Description	logFC	adj.P.Val
NM_001130037	ELMOD1	ELMO/CED-12 domain containing 1	2.178	0.0129
NM_014585	SLC40A1	solute carrier family 40 (iron-regulated transporter), member 1	1.499	0.0129
NM_000450	SELE	selectin E	1.486	0.0129
NM_001080396	FAM155A	family with sequence similarity 155, member A	1.370	0.0171
NM_001159995	NRG1	neuregulin 1	0.999	0.0258
NM_001127217	SMAD9	SMAD family member 9	1.111	0.0302
NM_001002796	MCTP1	multiple C2 domains, transmembrane 1	1.258	0.0348
NM_001077397	IRF2BP2	interferon regulatory factor 2 binding protein 2	0.949	0.0348
NM_005810	KLRG1	killer cell lectin-like receptor subfamily G, member 1	0.717	0.0348
NM_003856	IL1RL1	interleukin 1 receptor-like 1	1.648	0.0380
NM_024420	PLA2G4A	phospholipase A2, group IVA (cytosolic, calcium-dependent)	1.648	0.0380
NM_002165	ID1	inhibitor of DNA binding 1, dominant negative helix-loop-helix protein	1.560	0.0380
NM_004101	F2RL2	coagulation factor II (thrombin) receptor-like 2	1.437	0.0380
NM_021071	ART4	ADP-ribosyltransferase 4 (Dombrock blood group)	1.371	0.0380
NM_000963	PTGS2	prostaglandin-endoperoxide synthase 2 (prostaglandin G/H synthase and cyclooxygenase)	1.270	0.0380
NM_001204	BMPR2	bone morphogenetic protein receptor, type II (serine/threonine kinase)	0.884	0.0380
NM_001040665	STEAP2	STEAP family member 2, metalloreductase	0.661	0.0380
NM_001198999	SEMA6D	sema domain, transmembrane domain (TM), and cytoplasmic domain, (semaphorin) 6D	0.894	0.0406
NM_033425	DIXDC1	DIX domain containing 1	0.782	0.0421
NM_001080505	SHISA3	shisa family member 3	1.251	0.0422
ENST00000322813	FAM214B	family with sequence similarity 214, member B	0.741	0.0422
NM_000050	ASS1	argininosuccinate synthase 1	1.264	0.0449
NM_001005474	NFKBIZ	nuclear factor of kappa light polypeptide gene enhancer in B-cells inhibitor, zeta	0.899	0.0457
AK290080	HTR1B	5-hydroxytryptamine (serotonin) receptor 1B, G protein-coupled	0.609	0.0462
ENST00000424491	MRPL30	mitochondrial ribosomal protein L30	1.023	0.0462
ENST00000310613	SULT1B1	sulfotransferase family, cytosolic, 1B, member 1	0.885	0.0476
NM_001001323	ATP2B1	ATPase, Ca++ transporting, plasma membrane 1	0.751	0.0488
NM_014911	AAK1	AP2 associated kinase 1	0.575	0.0488
NM_001256426	PDLIM5	PDZ and LIM domain 5	0.705	0.0493
NM_006033	LIPG	lipase, endothelial	0.949	0.0497

Table E2 List of genes that are downregulated by pro-BMP9 following 5-hour treatment in PAECs. Microarray experiment is described in the Expanded Materials and Methods. Hits with adjusted P values less than 0.05 are shown.

Gene assignment	Gene name	Description	logFC	adj.P.Val
ENST00000300571	GPRC5B	G protein-coupled receptor, class C, group 5, member B	-1.349	0.0129
NM_000960	PTGIR	prostaglandin I2 (prostacyclin) receptor (IP)	-1.493	0.0129
NM_001190942	TNFSF10	tumor necrosis factor (ligand) superfamily, member 10	-1.522	0.0129
NM_003654	CHST1	carbohydrate (keratan sulfate Gal-6) sulfotransferase 1	-1.828	0.0129
NM_173567	EPHX4	epoxide hydrolase 4	-1.676	0.0129
NM_016580	PCDH12	protocadherin 12	-1.234	0.0171
NM_020808	SIPA1L2	signal-induced proliferation-associated 1 like 2	-1.135	0.0171
AK125058	ACSS1	acyl-CoA synthetase short-chain family member 1	-1.595	0.0173
ENST00000494111	FAM89A	family with sequence similarity 89, member A	-1.834	0.0173
NM_024576	OGFRL1	opioid growth factor receptor-like 1	-1.156	0.0173
NM_033274	ADAM19	ADAM metallopeptidase domain 19	-1.265	0.0173
NM_001145853	WFS1	Wolfram syndrome 1 (wolframin)	-1.037	0.0219
NM_001130158	MYO1B	myosin IB	-1.428	0.0225
NM_001003688	SMAD1	SMAD family member 1	-1.055	0.0254
NM_001280539	RNF19A	ring finger protein 19A, RBR E3 ubiquitin protein ligase	-0.921	0.0254
NM_001004196	CD200	CD200 molecule	-1.036	0.0288
NM_001136021	NFATC2	nuclear factor of activated T-cells, cytoplasmic, calcineurin-dependent 2	-1.476	0.0288
NM_002193	INHBB	inhibin, beta B	-2.006	0.0288
NM_003950	F2RL3	coagulation factor II (thrombin) receptor-like 3	-1.510	0.0288
NM_017413	APLN	apelin	-1.519	0.0288
XM_005266650	RNF152	ring finger protein 152	-1.031	0.0288
ENST00000525063	ADM	adrenomedullin	-1.317	0.0302
NM_001008540	CXCR4	chemokine (C-X-C motif) receptor 4	-2.332	0.0302
NM_001033910	TRAF5	TNF receptor-associated factor 5	-0.938	0.0302
NM_001099289	SH3RF3	SH3 domain containing ring finger 3	-0.768	0.0302
NM_001207012	PGF	placental growth factor	-1.533	0.0302
NM_006343	MERTK	MER proto-oncogene, tyrosine kinase	-0.846	0.0302
NM_006691	LYVE1	lymphatic vessel endothelial hyaluronan receptor 1	-0.862	0.0302
NM_007257	PNMA2	paraneoplastic Ma antigen 2	-0.881	0.0302
NM_014737	RASSF2	Ras association (RalGDS/AF-6) domain family member 2	-0.978	0.0302
NM_015253	WSCD1	WSC domain containing 1	-1.393	0.0302
NM_000222	KIT	v-kit Hardy-Zuckerman 4 feline sarcoma viral oncogene homolog	-2.092	0.0348
NM_001004354	NRARP	NOTCH-regulated ankyrin repeat protein	-1.115	0.0348
NM_001164211	LRCH1	leucine-rich repeats and calponin homology (CH) domain containing 1	-0.801	0.0348
NM_005308	GRK5	G protein-coupled receptor kinase 5	-0.820	0.0348
NM_014431	PALD1	phosphatase domain containing, paladin 1	-1.892	0.0348

NM_016545	IER5	immediate early response 5	-0.851	0.0348
NM_178172	GPIHBP1	glycosylphosphatidylinositol anchored high density lipoprotein binding protein 1	-0.886	0.0348
ENST00000282908	STK32B	serine/threonine kinase 32B	-0.805	0.0353
NM_006763	BTG2	BTG family, member 2	-1.029	0.0379
NM_018728	MYO5C	myosin VC	-1.003	0.0379
NM_000079	CHRNA1	cholinergic receptor, nicotinic, alpha 1 (muscle)	-0.948	0.0380
NM_001030060	SAMD5	sterile alpha motif domain containing 5	-0.746	0.0380
NM_001042481	FRMD6	FERM domain containing 6	-0.848	0.0380
NM_001098518	GPR116	G protein-coupled receptor 116	-0.956	0.0380
NM_001130861	CLDN5	claudin 5	-1.054	0.0380
NM_001134437	PHLDB2	pleckstrin homology-like domain, family B, member 2	-1.272	0.0380
NM_001143820	ETS1	v-ets avian erythroblastosis virus E26 oncogene homolog 1	-0.764	0.0380
NM_001164257	PRR29	proline rich 29	-1.055	0.0380
NM_001173977	LRRC16A	leucine rich repeat containing 16A	-0.922	0.0380
NM_001185061	AQP1	aquaporin 1 (Colton blood group)	-1.340	0.0380
NM_001204106	BCL2L11	BCL2-like 11 (apoptosis facilitator)	-1.711	0.0380
NM_001227	CASP7	caspase 7, apoptosis-related cysteine peptidase	-0.687	0.0380
NM_003884	KAT2B	K(lysine) acetyltransferase 2B	-0.717	0.0380
NM_012294	RAPGEF5	Rap guanine nucleotide exchange factor (GEF) 5	-0.722	0.0380
NM_003395	WNT9A	wingless-type MMTV integration site family, member 9A	-2.050	0.0381
NM_001178102	LOX	lysyl oxidase	-0.642	0.0390
NM_001029884	PLEKHG1	pleckstrin homology domain containing, family G (with RhoGef domain) member 1	-0.887	0.0394
NM_001146337	AFAP1L1	actin filament associated protein 1-like 1	-0.890	0.0394
NM_001251882	VIPR1	vasoactive intestinal peptide receptor 1	-0.980	0.0394
NM_002353	TACSTD2	tumor-associated calcium signal transducer 2	-0.756	0.0394
uc003ksx.1	SNCAIP	synuclein, alpha interacting protein	-2.222	0.0410
NM_001018009	SH3BP5	SH3-domain binding protein 5 (BTK-associated)	-0.826	0.0422
NM_001721	BMX	BMX non-receptor tyrosine kinase	-0.755	0.0422
NM_032206	NLRC5	NLR family, CARD domain containing 5	-0.871	0.0425
NM_000121	EPOR	erythropoietin receptor	-0.880	0.0437
NM_001257386	ABCG2	ATP-binding cassette, sub-family G (WHITE), member 2	-0.767	0.0449
NM_001128141	DPEP1	dipeptidase 1 (renal)	-0.606	0.0452
NM_001046	SLC12A2	solute carrier family 12 (sodium/potassium/chloride transporter), member 2	-0.713	0.0457
NM_001145652	C6orf141	chromosome 6 open reading frame 141	-1.039	0.0457
NM_007350	PHLDA1	pleckstrin homology-like domain, family A, member 1	-1.023	0.0457
NM_015111	N4BP3	NEDD4 binding protein 3	-1.818	0.0462
NM_005077	TLE1	transducin-like enhancer of split 1 (E(sp1) homolog, Drosophila)	-0.742	0.0466
NM_013296	GPSM2	G-protein signaling modulator 2	-0.762	0.0466
NM_153208	IQCK	IQ motif containing K	-0.698	0.0466

NM_001282431	ARL4C	ADP-ribosylation factor-like 4C	-0.772	0.0472
NM_018288	PHF10	PHD finger protein 10	-0.654	0.0475
NM_014059	RGCC	regulator of cell cycle	-1.106	0.0480
NM_001025109	CD34	CD34 molecule	-1.289	0.0488
NM_014239	EIF2B2	eukaryotic translation initiation factor 2B, subunit 2 beta, 39kDa	-0.597	0.0488
NM_014909	VASH1	vasohibin 1	-0.614	0.0488
NM_001142621	TGFBRAP1	transforming growth factor, beta receptor associated protein 1	-0.923	0.0493
NM_006558	KHDRBS3	KH domain containing, RNA binding, signal transduction associated 3	-1.074	0.0493
NM_005092	TNFSF18	tumor necrosis factor (ligand) superfamily, member 18	-0.826	0.0497
OTTHUMT00000322250	RIBC2	RIB43A domain with coiled-coils 2	-0.734	0.0497

Table E3. Summary of pathway analysis of BMP9 regulated protein-protein interaction (PPI) network. In the microarray analysis, we used N=4 hPAEC lines (isolated from four different individuals), and at a single time point, 5 hours. The continuum changes in the adjusted *P*-values (adj *P*) for differentially regulated genes indicate that the up and down regulated genes are likely to be more than those passing the adj $P < 0.05$ threshold, and the reasons for not reaching the adj *P* of 0.05 cut-off could be due to either the sample number was too small, or the peak time for the change is not at 5 hours. Therefore, we have performed the PPI network analysis using the gene set with adj *P*-value cut-off at 0.05, 0.06 and 0.08. The analysis was performed using STRING(13). The network stats summaries of all analyses are shown below, enriched pathways shown in Supplemental Table E2, enriched cellular components shown in Table E3 and Network view of differentially regulated genes shown in Supplemental Figure E2.

Changes in gene expression	number of nodes	number of edges	expected number of edges	PPI enrichment *P*-value
Adj P <0.05				
up and down	98	67	26	2.06E-11
up only	26	6	1	0.003
down only	72	35	15	8.52E-06
Adj $P < 0.06$				
up and down	123	93	37	9.77E-15
up only	33	12	2	6.60E-06
down only	90	44	20	3.33E-06
Adj $P < 0.08$				
up and down	156	133	55	<1.0e-16
up only	46	18	5	8.93E-06
down only	110	55	26	3.40E-07

Table E4. Summary of enriched pathways in hPAECs from pathway analysis of BMP9 regulated PPI network.

Changes in gene expression	enriched pathways	count in gene set	false discovery rate
Adj P <0.05			
up and down	TGFβ signaling pathway	5	0.00982
	cytokine-cytokine receptor interaction	7	0.0367
	Rap1 signaling pathway	6	0.043
	Hippo signaling pathway	5	0.0494
up only	Mineral absorption	3	0.00927
	TGFβ signaling pathway	3	0.018
down only	no enriched pathways detected		
Adj P < 0.06			
up and down	TGFβ signaling pathway	6	0.00201
	Rap1 signaling pathway	7	0.0226
	cytokine-cytokine receptor interaction	8	0.0226
	VEGF signaling pathway	4	0.0315
up only	TGFβ signaling pathway	4	0.00201
	Mineral absorption	3	0.00961
down only	Rap1 signaling pathway	6	0.0407
	cytokine-cytokine receptor interaction	7	0.0407
Adj P < 0.08			
up and down	TNF signaling pathway	8	0.000439
	Rap1 signaling pathway	9	0.00229
	cytokine-cytokine receptor interaction	10	0.00229
	TGFβ signaling pathway	6	0.00229
	microRNAs in cancer	6	0.0464
up only	TGFβ signaling pathway	4	0.00771
	TNF signaling pathway	4	0.0135
	Mineral absorption	3	0.0174
	MicroRNAs in cancer	4	0.0213
down only	Rap1 pathway	7	0.0339

Table E5 Summary of enriched cellular component gene ontology analysis in hPAECs from pathway analysis of BMP9 regulated PPI network

Pathway ID	Pathway description	Count in gene set	False discovery rate
GO:0045177	Apical part of cell	12	0.000585
GO:0098589	Membrane region	21	0.000585
GO:0005615	Extracellular space	22	0.000769
GO:0031226	Intrinsic component of plasma membrane	25	0.000769
GO:0098590	Plasma membrane region	18	0.000769
GO:0005887	Integral component of plasma membrane	24	0.000789
GO:0071944	Cell periphery	48	0.000789
GO:0005886	Plasma membrane	47	0.000992
GO:0045178	Basal part of cell	5	0.00165
GO:0031224	Intrinsic component of membrane	53	0.00179

Table E6. Patient demographics and clinical parameters. Enrolled subjects were characterized as systemic inflammatory response syndrome (SIRS) or sepsis by a group of blinded critical care physicians(14), or were healthy controls. A subset of randomly selected subjects from the MICU Registry with the above diagnoses was selected for analysis. Anonymized plasma samples were generated from blood collected in EDTA-containing tubes obtained from patients within 24 to 72 hours of MICU admission and stored at –80°C. Plasma was isolated from whole blood at 1500 *g* for 15 minutes at room temperature.

Variable	**Control (n=10)**	**SIRS (n =10)**	**Sepsis (n=10)**	***P* value ǁ**	**Statistical test**
Age (yr)*	56 [28, 80]	56 [28, 74]	64 [41, 92]	0.1364	ANOVA with Tukey
Gender, n (%)				0.8663	Chi square
-Female	4 (40)	4 (40)	3 (30)		
-Male	6 (60)	6 (60)	7 (70)		
Race, n (%)				0.3126	Chi square
-White	8 (80)	6 (60)	8 (80)		
-Black	0 (0)	2 (20)	0 (0)		
-Hispanic	0 (0)	1 (10)	1 (10)		
-American Indian/Alaskan native	0 (0)	1 (10)	0 (0)		
-Asian/Pacific Islander	2 (20)	0 (0)	1 (10)		
Positive cultures, n (%)	N/A	0 (0)	9 (90)	<0.0001	Chi square (0.0001 by Fisher's exact)
Vasopressors within 24 hr of admission, n (%)	N/A	2 (20)	9 (90)	0.0017	Chi square (0.0055 by Fisher's exact)
Mechanical ventilation within 24 hr of admission, n (%)	N/A	3 (30)	2 (20)	0.6056	Chi square (>0.9999 by Fisher's exact)
Acute Physiology and Chronic Health Evaluation (APACHE) II score*	N/A	25 [10, 34]	23 [19, 31]	0.6610	Unpaired t test
Sequential Organ Failure Assessment (SOFA) score*	N/A	17 [4, 20]	18 [13, 24]	0.2681	Mann Whitney
Comorbidities, n (%)				N/A	
-Coronary artery disease	0 (0)	1 (10)	3 (30)		
-Congestive heart failure	0 (0)	0 (0)	1 (10)		
-Chronic obstructive pulmonary disease	0 (0)	1 (10)	1 (10)		
-Diabetes mellitus	0 (0)	5 (50)	2 (20)		
-Liver disease	0 (0)	3 (30)	0 (0)		
-Chronic kidney disease	0 (0)	2 (20)	3 (30)		
-Cancer	1 (10)	4 (40)	5 (50)		
-Solid tumor	1 (10)	2 (20)	1 (10)		
-Hematologic	0 (0)	2 (20)	4 (40)		
-Bone marrow transplant	0 (0)	1 (10)	2 (20)		

Creatinine† (mean+/-SD)	N/A	2.4 ± 3.0	2.4 ± 1.8	0.3930	Mann Whitney
Lactate† (mean+/-SD)	N/A	4.3 ± 4.1‡	2.5 ± 1.2§	0.9747	Mann Whitney

N/A Not applicable
* Age, Acute Physiology and Chronic Health Evaluation (APACHE) II, and Sequential Organ Failure Assessment (SOFA) scores are expressed in medians [min, max 95% CI]. All other values are expressed by percentage of total of subjects (in parentheses) and total number.
† Highest value within the first 24 hours upon admission to the ICU. Creatinine units are given in mg/dL, Lactate units are given in mEq/L. Data are presented mean ± sd.
‡ $n = 6$
§ $n = 8$
|| P values reflect overall comparison of the groups with existing data

Supplemental References:

1. Jiang H, Salmon RM, Upton PD, Wei Z, Lawera A, Davenport AP, Morrell NW, Li W. The Prodomain-bound Form of Bone Morphogenetic Protein 10 Is Biologically Active on Endothelial Cells. *J Biol Chem* 2016; 291: 2954-2966.
2. Salmon RM, Guo J, Wood JH, Tong Z, Beech JS, Lawera A, Yu M, Grainger DJ, Reckless J, Morrell NW, Li W. Molecular basis of ALK1-mediated signalling by BMP9/BMP10 and their prodomain-bound forms. *Nat Commun* 2020; 11: 1621.
3. Owen-Woods C, Joulia R, Barkaway A, Rolas L, Ma B, Nottebaum AF, Arkill KP, Stein M, Girbl T, Golding M, Bates DO, Vestweber D, Voisin MB, Nourshargh S. Local microvascular leakage promotes trafficking of activated neutrophils to remote organs. *J Clin Invest* 2020; 130: 2301-2318.
4. Woodfin A, Voisin MB, Beyrau M, Colom B, Caille D, Diapouli FM, Nash GB, Chavakis T, Albelda SM, Rainger GE, Meda P, Imhof BA, Nourshargh S. The junctional adhesion molecule JAM-C regulates polarized transendothelial migration of neutrophils in vivo. *Nat Immunol* 2011; 12: 761-769.
5. Hoenderdos K, Lodge KM, Hirst RA, Chen C, Palazzo SG, Emerenciana A, Summers C, Angyal A, Porter L, Juss JK, O'Callaghan C, Chilvers ER, Condliffe AM. Hypoxia upregulates neutrophil degranulation and potential for tissue injury. *Thorax* 2016; 71: 1030-1038.
6. Livak KJ, Schmittgen TD. Analysis of relative gene expression data using real-time quantitative PCR and the 2(-Delta Delta C(T)) Method. *Methods* 2001; 25: 402-408.
7. Matute-Bello G, Downey G, Moore BB, Groshong SD, Matthay MA, Slutsky AS, Kuebler WM, Acute Lung Injury in Animals Study G. An official American Thoracic Society workshop report: features and measurements of experimental acute lung injury in animals. *Am J Respir Cell Mol Biol* 2011; 44: 725-738.
8. Long L, Ormiston ML, Yang X, Southwood M, Graf S, Machado RD, Mueller M, Kinzel B, Yung LM, Wilkinson JM, Moore SD, Drake KM, Aldred MA, Yu PB, Upton PD, Morrell NW. Selective enhancement of endothelial BMPR-II with BMP9 reverses pulmonary arterial hypertension. *Nat Med* 2015; 21: 777-785.
9. Carvalho BS, Irizarry RA. A framework for oligonucleotide microarray preprocessing. *Bioinformatics* 2010; 26: 2363-2367.
10. Irizarry RA, Hobbs B, Collin F, Beazer-Barclay YD, Antonellis KJ, Scherf U, Speed TP. Exploration, normalization, and summaries of high density oligonucleotide array probe level data. *Biostatistics* 2003; 4: 249-264.
11. Ritchie ME, Phipson B, Wu D, Hu Y, Law CW, Shi W, Smyth GK. limma powers differential expression analyses for RNA-sequencing and microarray studies. *Nucleic Acids Res* 2015; 43: e47.
12. Benjamini Y, Hochberg Y. Controlling the false discovery rate - a practical and powerful approach to multiple testing. *Journal of the Royal Statistical Society Series B - Methodological* 1995; 57: 289-300.
13. Szklarczyk D, Franceschini A, Wyder S, Forslund K, Heller D, Huerta-Cepas J, Simonovic M, Roth A, Santos A, Tsafou KP, Kuhn M, Bork P, Jensen LJ, von Mering C. STRING v10: protein-protein interaction networks, integrated over the tree of life. *Nucleic Acids Res* 2015; 43: D447-452.
14. Levy MM, Fink MP, Marshall JC, Abraham E, Angus D, Cook D, Cohen J, Opal SM, Vincent JL, Ramsay G, Sccm/Esicm/Accp/Ats/Sis. 2001 SCCM/ESICM/ACCP/ATS/SIS International Sepsis Definitions Conference. *Crit Care Med* 2003; 31: 1250-1256.

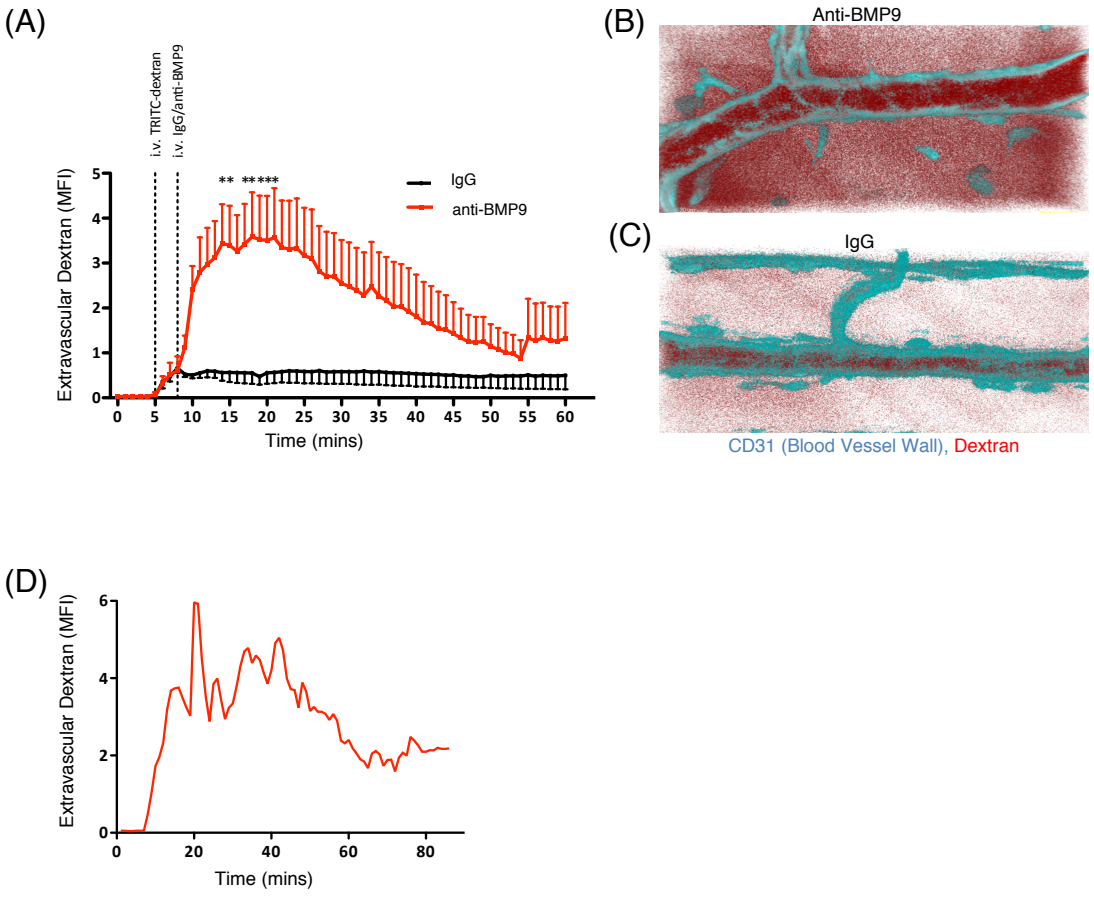

Figure E1. Intravital confocal microscopy tracking the microvascular leak *in vivo* after neutralizing endogenous BMP9. Anti-CD31-AF647 was injected intrascrotally 2 hours before imaging to label the blood vessel walls. Three minutes after intravenous infusion of TRITC-dextran, anti-BMP9 or IgG control was infused intravenously and the vessel imaged continuously for 1 hour to monitor vascular leakage. (A) Data illustrating the kinetics of microvascular leakage following anti-BMP9 (red) or control IgG (black) administration, N=3. Data are presented as mean fluorescence intensity (MFI) of extravasated dextran found within 50 μm of the venular wall. Two-way repeated measures ANOVA plus Bonferroni post hoc test, *, $P < 0.05$ compared to matched time point in control group. (B&C) Representative images illustrating enhanced dextran extravasation into extravascular tissue 5 minutes following anti-BMP9 (B) or IgG control (C) infusion. Note that perivascular macrophages sometimes appear CD31-positive. (D) Kinetics of microvascular leakage following histamine (2.25 μmoles) administration.

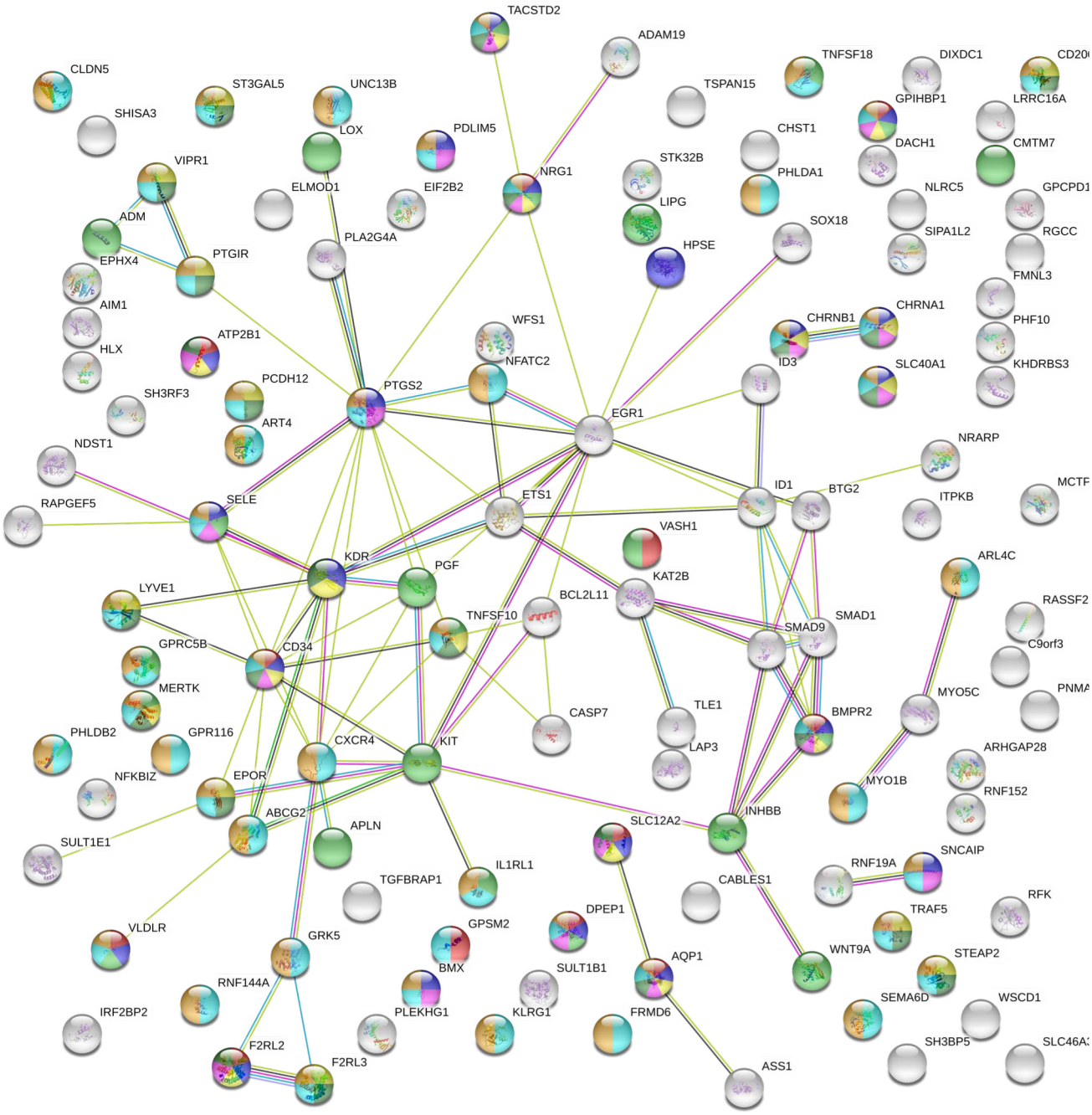

Figure E2. BMP9 regulated genes are highly enriched on plasma membrane or extracellular space. Protein-protein interactions network of differential regulated genes by BMP9 (using adj P-value of 0.06 cutoff, Table E3). Figure generated using STRING Sever (https://string-db.org/).

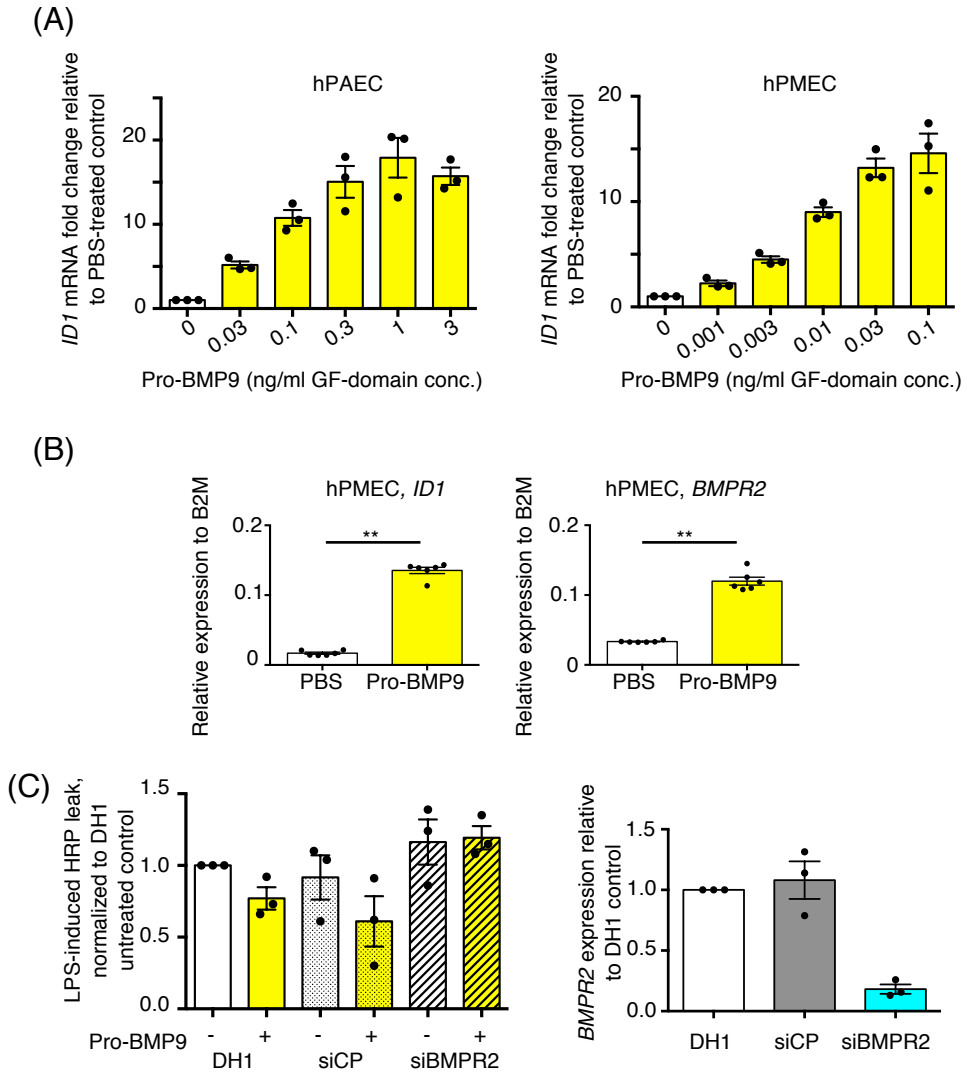

Figure E3. BMP9 signaling in hPMECs. (A) Dose-dependent pro-BMP9 signalling in PAECs and PMECs. Cells were quiesced in EGM-2/0.1% FBS overnight and treated with pro-BMP9 at indicated dose for 1.5 hours before harvested for RNA extraction and RT-qPCR analysis. N=3 independent experiments, means ± SEM are shown. (B) PMECs were treated with pro-BMP9 or PBS for 1.5 hours (for *ID1* gene expression) or 5 hours (for *BMPR2* gene expression) before cells were harvested for RT-qPCR analysis. N=6 independent experiments. Means ± SEM are shown, Two tailed, Mann-Whitney test. **, $P < 0.01$. (C) Protection of LPS-induced permeability by BMP9 is BMPR-II dependent. BMPR2 was knockdown using siRNA in PMECs. 24 hours later, cells were seeded in transwell insert and grown for 48 hours before subject to LPS-induced permeability assays as described in the online method. Three independent siRNA knock down experiments followed by permeability assays were performed. Left, Leaked HRP activity normalized to DH1 without BMP9. Right, qPCR showing the siRNA efficiency. Data shown as means ± SEM of three independent experiments.

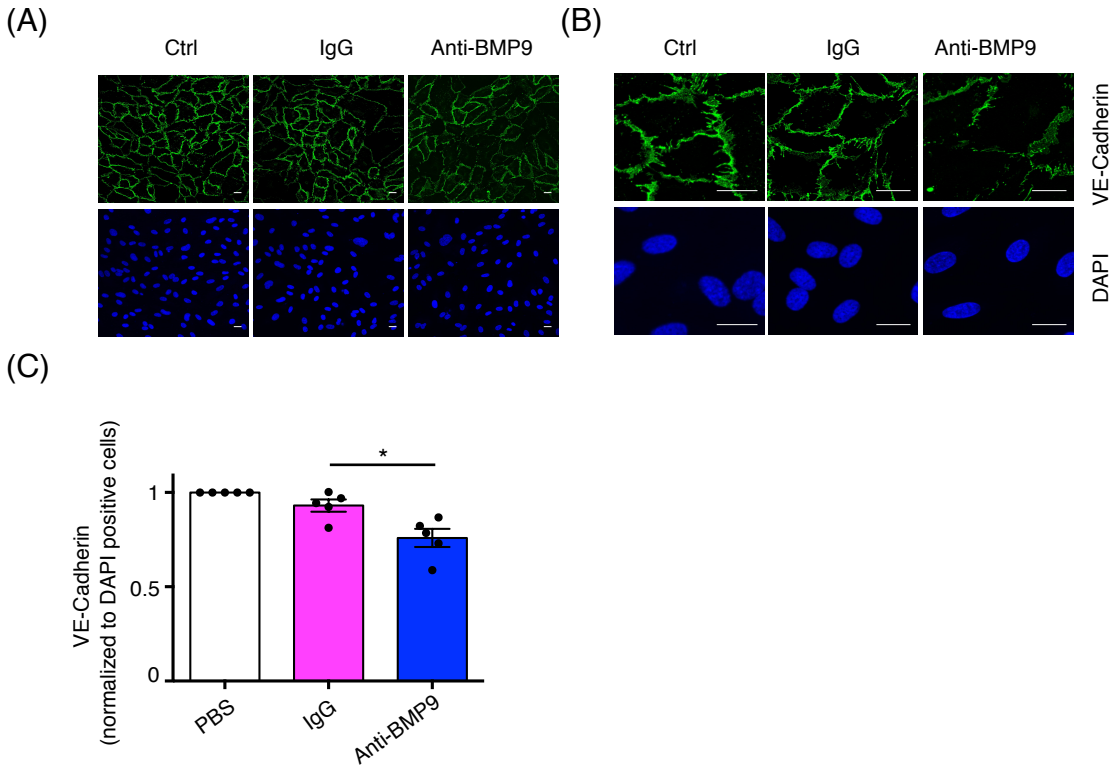

Figure E4. Selective inhibiting BMP9 in endothelial growth media leads to a rapid loss of VE-cadherin junctions in PAECs. (A&B) Low- and High-powered confocal images of hPAECs stained with VE-cadherin (green) or DAPI (Blue), following 15-minutes treatment with PBS, anti-BMP9 or IgG isotype control. Scale bars = 20 μM. (C) Quantification of VE-cadherin staining from low-powered images as described in the on-line expanded methods. Means ± SEM are shown, two-tailed Mann-Whitney test, *, $P <$ 0.05.

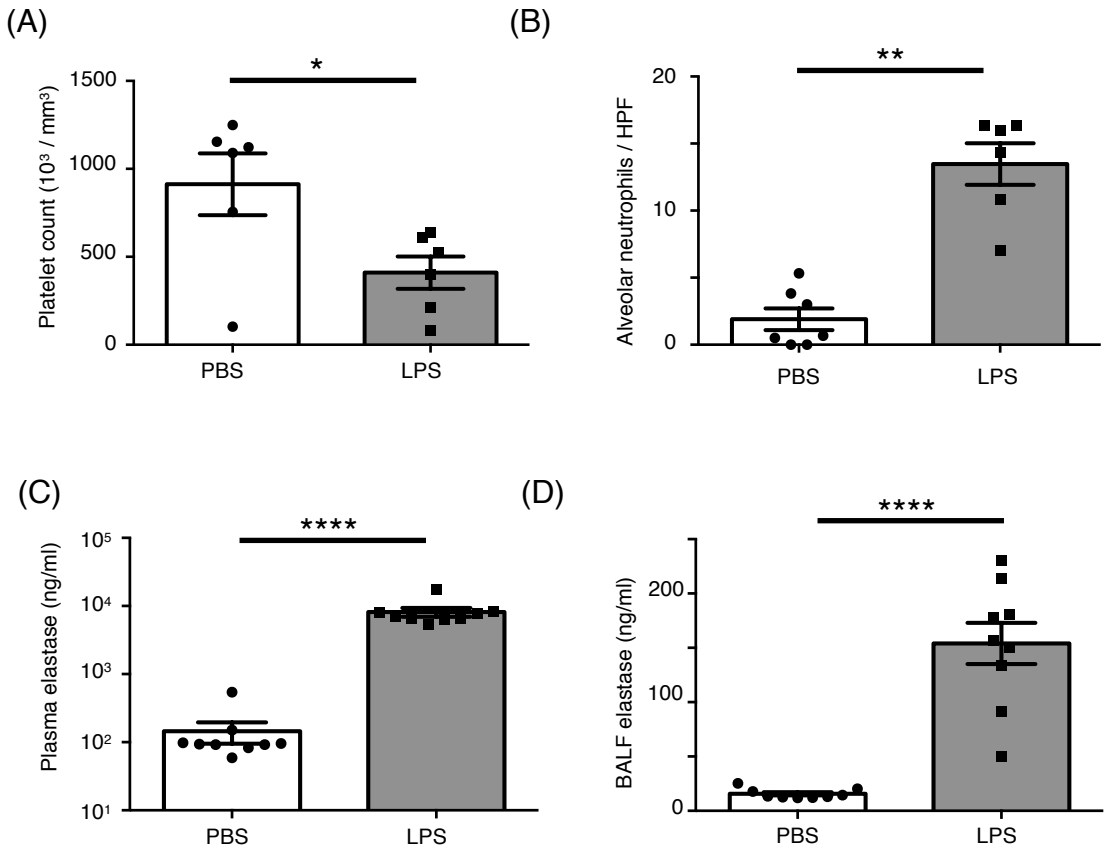

Figure E5. Murine model of endotoxemia induced by acute intraperitoneal LPS challenge. (A) Full blood count, showing % platelet counts were decreased in the LPS-treated animals. N=6 in each group. (B) Alveolar neutrophils were increased in the mice treated with LPS. (C&D) Elastase concentrations in plasma and BALF measured by ELISA. N=9. Data shown as means ± SEM. Two-tailed, Mann-Whitney test, *, $P < 0.05$; ****, $P < 0.0001$.

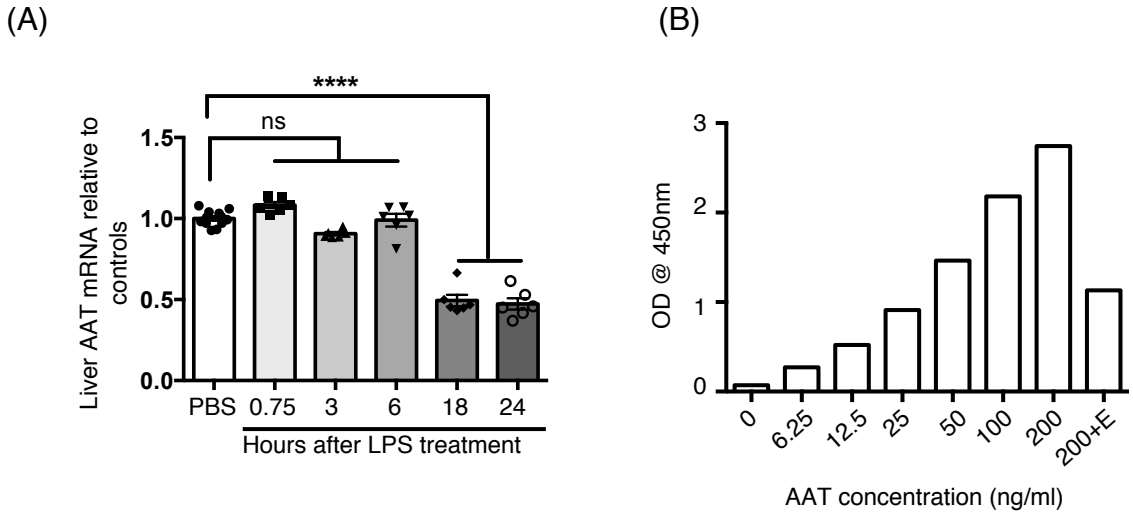

Figure E6. The regulation of endogenous BMP9 during endotoxemia: additional AAT measurements. (A) Changes in liver AAT mRNA relative to controls after LPS challenge. One-way ANOVA, Tukey's post-test. ****, $P < 0.0001$. (B) Mouse AAT ELISA kit only detects native AAT. Upon adding the elastase to the standard (200+E), the signal decreased, probably due to the large conformational change in AAT upon elastase cleavage.